New insights on the distribution of interlayer water in bi-hydrated smectite from X-ray diffraction profile modeling 00l reflections

Eric Ferrage, Bruno Lanson, Natalie Malikova, Alain Plançon, Boris.A. Sakharov, Victor.A. Drits

New insights on the distribution of interlayer water in bi-hydrated smectite from X-ray diffraction profile modeling of 00ℓ reflections

Eric Ferrage[1,2], Bruno Lanson[1,*], Natalie Malikova[2,3], Alain Plançon[4], Boris A. Sakharov[1,5], and Victor A. Drits[1,5]

[1] Environmental Geochemistry Group, LGIT – Maison des Géosciences, Joseph Fourier University – CNRS, BP53, F-38041 Grenoble cedex 9, France

[2] ANDRA, Parc de la Croix Blanche, 1-7 rue Jean Monnet, F-92298 Châtenay-Malabry cedex, France

[3] Laboratory Liquides Ioniques & Interfaces Chargées, Paris 06 University, Case Courrier 51, 4 Pl. Jussieu, F-75252 Paris; France

[4] Crystallography Laboratory, ISTO, University of Orléans - CNRS, F-45067 Orléans Cedex 2, France.

[5] Geological Institute, Russian Academy of Sciences, 7 Pyzhevsky street, 109017 Moscow, Russia

* Author to whom correspondence should be addressed.

e-mail : Bruno.Lanson@obs.ujf-grenoble.fr

Abstract

The interlayer configuration proposed by Moore and Reynolds and commonly used to reproduce the 00ℓ reflections of bi-hydrated smectite is shown to be inconsistent with experimental X-ray diffraction data.[1] The alternative configuration of interlayer species with cations located in the mid-plane of the interlayer and one sheet of H_2O molecules on each side of this plane is also shown to imperfectly describe the actual structure of bi-hydrated smectites. Specifically, the thermal fluctuation of atomic positions (Debye-Waller factor) used to describe the positional disorder of interlayer H_2O molecules has to be increased to unrealistic values to satisfactorily reproduce experimental X-ray diffraction data when using this model. A new configuration is thus proposed for the interlayer structure of bi-hydrated smectite. Cations are located in the mid-plane of the interlayer whereas H_2O molecules are scattered about two main positions according to Gaussian-shaped distributions. This configuration allows reproducing all 00ℓ reflections with a high precision, with only one new variable parameter (width of the Gaussian function). The proposed configuration is consistent with those derived from Monte-Carlo calculations and allows matching more closely the amount of interlayer water that can be determined independently from water vapor adsorption/desorption isotherm experiments. In addition, the proposed configuration of interlayer species appears valid for both dioctahedral and trioctahedral smectites exhibiting octahedral and tetrahedral substitutions, respectively, thus not allowing to differentiate these expandable 2:1 phyllosilicates from their respective interlayer configuration.

Introduction

Smectite is a 2:1 phyllosilicate whose layer structure consists of an octahedral sheet sandwiched in-between two siliceous tetrahedral sheets. Isomorphic substitutions in either tetrahedral or octahedral sites induce a permanent negative layer charge, which is compensated for by the presence of hydrated cations in the interlayer. The observation of 00ℓ basal reflections on X-ray diffraction (XRD) patterns has shown that with increasing relative humidity smectite expands stepwise, the different steps corresponding to the intercalation of 0, 1, 2 or 3 sheets of H_2O molecules in the interlayer.[2-6] From these pioneer studies, it is now commonly accepted that the expandability of 2:1 phyllosilicates is controlled by factors such as the nature of interlayer cations, and the layer charge and its location (octahedral vs. tetrahedral). These general observations have led to different models in which crystalline swelling is controlled by the balance between the repulsive forces between neighboring 2:1 layers and the attractive forces between hydrated interlayer cations and the negatively-charged surface of siloxane sheets.[6-11]

The development of XRD modeling techniques allowed investigating structures in which different hydration states coexist thus improving these early observations.[12-17] Ferrage et al. used such a modeling approach to characterize the hydration of several montmorillonite and beidellite samples and observed that the nature of the interlayer cation, and in particular its affinity for water, influences the layer thickness of bi-hydrated and monohydrated layers.[18,19] They also confirmed that the relative proportions of the different layer types, which correspond to the different hydration states, depend on both the amount and the location of smectite layer charge. In addition, these authors showed that XRD peak profiles and position can be satisfactorily reproduced, especially over the low-angle region (~5-12°2θ Cu Kα), only if hydration heterogeneity is taken into account. They were thus able to refine

69 the structure of smectite and in particular to investigate atomic positions of interlayer species.
70 In particular, they showed that the atomic positions reported by Moore and Reynolds for H_2O
71 molecules in bi-hydrated layers induce a dramatic misfit over the medium- to high-angle
72 region (12-50°2θ Cu Kα) by strongly modifying the intensity ratio between the different 00ℓ
73 reflections.[1,18]

74 The present article thus aims at refining further the structure of interlayer H_2O in bi-
75 hydrated smectites from the fit of experimental XRD patterns. The proposed structure is
76 compared with the positional distribution commonly derived from Monte-Carlo simulations,
77 whereas the adjusted amounts of interlayer water are compared with those determined
78 experimentally from water vapor adsorption-desorption experiments.

79

80 ## Background

81

82 **Smectite hydration heterogeneity as seen by XRD profile modeling.** In agreement
83 with the stepwise evolution of the d_{001} basal spacing on XRD patterns, the hydration state of
84 smectite has been described using three layer types exhibiting different layer thickness
85 corresponding to the common hydration states reported for montmorillonite in non-saturated
86 conditions. Dehydrated layers (0W – Layer thickness ~9.6-10.1 Å), mono-hydrated layers
87 (1W – Layer thickness ~12.3-12.7 Å), and bi-hydrated layers (2W – Layer thickness ~15.1-
88 15.8 Å) have thus been defined. In the first two layer types, interlayer cations are located in
89 the mid-plane of the interlayer, together with H_2O molecules for 1W layers. For 2W layers,
90 interlayer cations are also commonly assumed to be located in the mid-plane of the
91 interlayer.[1] In addition, it is usually assumed that two planes of H_2O molecules, each bearing
92 0.69 H_2O per $O_{20}(OH)_4$, are located at 0.35 and 1.06 Å from the cation along the c* axis
93 (Debye-Waller parameter B_{wat} ~2 $Å^2$ for these two planes), whereas a third denser plane (1.20

H_2O per $O_{20}(OH)_4$) is located further from the central interlayer cation at 1.20 Å along the c* axis (B_{wat} = 11 $Å^2$).[1] The pattern calculated for the Ca-saturated reference SWy-1 montmorillonite (Ca-SWy-1) assuming a homogeneous 2W hydration state and the above configuration for interlayer species is compared on Figure 1a to the experimental pattern recorded at 80% RH. With these usual hypotheses, the calculated pattern fits most of the experimental pattern features but significant discrepancies can be observed over the medium- to the high-angle region in spite of the low intensity diffracted. In particular, the position of the 005 reflection and the low-angle "tail" of the 002 reflection are not well reproduced (Figure 1a). Ferrage et al. challenged this usual configuration of interlayer species, and proposed an alternative configuration that includes a unique plane of H_2O molecules located at 1.20 Å, along the c* axis, on either side of the central interlayer cation (2WS configuration).[18] The use of this 2WS configuration helps reducing the discrepancies observed for the 003-005 reflections. In particular, this configuration allows decreasing the relative intensity of the 003 and 004 reflections whereas the intensity of the 005 one is increased (Figure 1b). However, in the high-angle region the intensity ratio between the 007 and 008 reflections measured on the calculated pattern is inconsistent with that determined experimentally, although the intensity of the 008 reflection is correctly reproduced.

Ferrage et al. also demonstrated that the common hypothesis of a homogeneous hydration state for smectite is not consistent with the likely existence in smectite of structural heterogeneities affecting the layer charge distribution (from one interlayer to the other or within a given interlayer) and/or location (octahedral vs. tetrahedral).[18] In turn these heterogeneities lead to the coexistence of different layer types in a single structure. Such hydration heterogeneity has been evidenced from the profile modeling of XRD patterns recorded on hydrated smectites.[12-17] Ferrage et al. have shown that this heterogeneity is systematically observed whatever the interlayer cation, the relative humidity (RH), and the

119 amount and location of the layer charge deficit.[18,19] It is thus essential to account for the
120 hydration heterogeneity to satisfactorily reproduce the experimental positions and profiles of
121 reflections.

122 Ferrage et al. have shown indeed that accounting for smectite hydration heterogeneity
123 allows fitting better the profiles of all experimental 00ℓ reflections.[18,19] In particular
124 heterogeneous samples were modeled by combining the contributions of several structures,
125 each containing either one (periodic structure) or different layer types (mixed-layer structure –
126 MLS) randomly interstratified (R=0).[18-20] These different contributions should be seen as a
127 simplified way to describe the actual hydration heterogeneity of the sample under
128 investigation, with the different layer types not being distributed at random in the different
129 crystallites. However, the coexistence of these contributions does not imply the actual
130 presence of populations of particles in the sample, as their relative proportions may vary as a
131 function of RH for example.[18] To account for the heterogeneous distribution of the different
132 layer types within smectite crystallites, layers exhibiting the same hydration state that are
133 present in the different MLSs must have identical properties as they may be accounted for in
134 one or the other structure depending on the RH. In particular for a given XRD pattern, each
135 layer type must possess a constant crystal-chemistry in the different MLSs. It was possible to
136 reproduce the profile of all experimental 00ℓ reflections of the experimental XRD pattern
137 recorded on Ca-SWy-1 at 80% RH by considering two MLSs (Figure 1c) and the 2WS
138 configuration for interlayer water.[18] Specifically, the position of the 005 reflection, the low-
139 angle shoulder of the 002 reflection and the "tails" of the 001 reflection are satisfactorily
140 reproduced by taking hydration heterogeneity into account. Accounting for hydration
141 heterogeneity also helps reproducing the relative intensity of higher-angle reflections (002,
142 003, 004, and 005 for example) but significant discrepancies that could result from an
143 incorrect structure model for interlayer water are still visible for high-angle reflections (Figure

144 1c). Specifically, the 006, 007 and 008 reflections are not satisfactorily reproduced, as for
145 example the intensity ratio between the 007 and 008 reflections measured on experimental
146 and calculated patterns are inconsistent. These discrepancies are reduced by increasing the
147 Debye-Waller factor of H_2O molecules (B_{wat}) from 2 to 11 $Å^2$ for this 2WS configuration of
148 interlayer H_2O molecules (Figure 1d).[18] However, such high values of the Debye-Waller
149 factor are not sufficient to conceal the disagreement for the intensity ratio between 007 and
150 008 reflections, and thermal atomic fluctuations most likely do not adequately describe the
151 positional distribution of H_2O molecules in 2W smectite layers, and additional hypotheses
152 have to be sought.

153 **Interlayer configuration of 2W smectite layers as seen by Monte-Carlo**
154 **simulations**. In the above calculations, H_2O molecules are distributed in discrete planes, and
155 the positional distribution of H_2O molecules results only from their thermal motion. However,
156 this simplified description of the smectite interlayer structure does not allow fitting the
157 experimental XRD data (Figures 1c, 1d) most likely because the description of H_2O molecule
158 positional disorder is incomplete. A more complete (realistic ?) description of the interlayer
159 structure may be obtained from Monte-Carlo (MC) simulations which allow taking into
160 account all interactions among interlayer species, as well as between these species and the 2:1
161 layer.[21] It is in particular possible to account for the hydration variability of interlayer cation
162 which can form either inner-sphere or outer-sphere complexes with the 2:1 layer surface,
163 leading to the existence or to the lack, respectively, of direct interactions with O atoms from
164 the layer surface. In the latter case, these interactions are screened by H_2O molecules from the
165 cation hydration sphere. It has been shown that, as compared to other monovalent cations, K^+
166 cations tend to form inner-sphere complexes in montmorillonite interlayers and that these
167 cations remain partially bound to the 2:1 clay surface even in the 2W state.[22,23] On the
168 contrary, Li^+ and Na^+ cations in 2W smectites are located in the mid-plane of the interlayer.[23-

169 The location of the layer charge deficit has also been shown to influence the hydration of
170 interlayer Na^+ cations, the formation of inner-sphere complexes being favored by tetrahedral
171 substitutions.[26] On the other hand, a majority of interlayer Na^+ cations is located in the mid-
172 plane of the interlayer for octahedrally substituted 2W smectites.[23,24] A similar influence of
173 the charge location was reported for K- and Li-saturated 2W smectites.[22,25] In contrast,
174 whatever the charge location Mg^{2+} cations are systematically octahedrally coordinated in 2W
175 smectites and located in the mid-plane of the interlayer.[27,28] In any case, MC simulations most
176 often indicate that H_2O molecules do not form a discrete plane but rather show that they are
177 distributed about a "most probable" position. In addition, the mixed charge location common
178 in smectite layers, and more especially in those of natural samples, can lead to the coexistence
179 in a single smectite interlayer of different complexes, thus broadening the water distribution
180 profile by perturbing the hydrogen bond network and the orientation of the water dipole.[29]
181 Even though MC simulations do not commonly account for smectite hydration heterogeneity,
182 which is best revealed by XRD analysis, such a description of H_2O molecules positional
183 disorder could be the missing link toward a better structure determination of H_2O
184 configuration in 2W smectite layers.
185

186 **Materials and Methods**

187

188 **Experimental**. Samples investigated in the present work include two reference low-
189 charge montmorillonites (SWy-1 and SWy-2) available from the Source Clays Repository
190 (http://www.agry.purdue.edu/cjohnston/sourceclays/index.html) and two synthetic saponite
191 samples. The latter samples were selected because of their contrasting layer charges (0.8 and
192 1.4 per $O_{20}(OH)_4$).[30,31] The size fractionation of all samples, and their homoionic saturation
193 were performed as described by Ferrage et al.[18] For all samples, oriented slides were prepared

by drying at room temperature a clay slurry pipetted onto a glass slide. XRD patterns were then recorded using a Bruker D5000 diffractometer equipped with a Kevex Si(Li) solid-state detector, an Ansyco rh-plus 2250 humidity control device coupled to an Anton Paar TTK450 chamber. Usual scanning parameters were 0.04°2θ as step size and 6s as counting time per step over the 2-50°2θ Cu Kα angular range. The divergence slit, the two Soller slits, the antiscatter and resolution slits were 0.5°, 2.3°, 2.3°, 0.5° and 0.06°, respectively. Data collection conditions (60 and 80% RH for Sr-saturated samples, 40 and 80% RH for Ca-saturated samples, and 80 or 90% RH for Na-saturated samples) were selected because of the high amount of 2W layers (>90%) present in these conditions.[18]

Simulation of X-ray diffraction data. The algorithms developed initially by Drits and coworkers were used to fit experimental XRD profiles over the 2–50°2θ CuKα range using a trial-and-error approach.[32-34] Instrumental and experimental factors such as horizontal and vertical beam divergences, goniometer radius, length and thickness of the oriented slides were measured and introduced without further adjustment. The mass absorption coefficient (μ^*) was set to 45 cm^2g^{-1}, as recommended by Moore and Reynolds,[1] whereas the parameter characterizing the preferred orientation of the particles in the sample (σ^*) was considered as a variable parameter. Additional variable parameters include the coherent scattering domain size (CSDS) along the c* axis which was characterized by a maximum CSDS value, set to 45 layers, and by a variable mean CSDS value (N).[35] In addition, because of the weak bonds between adjacent smectite layers, layer thickness was allowed to deviate from the average d_{001} value. This cumulative deviation from periodicity, which is described as a "disorder of the second type",[36,37] is accounted for by introducing a variance parameter σ_z.[18] z-coordinates of all atoms building up the 2:1 layer framework as well as those present in the interlayer of 0W and 1W layers were set as proposed by Moore and Reynolds.[1] The interlayer structure of 2W layers has been refined to account for all features of experimental XRD patterns recorded on

219 2W-dominated samples. In particular, a double Gaussian distribution of H_2O molecules along
220 the c* axis (2WG) was assumed. This 2WG model accounts both for the presence of a unique
221 plane of H_2O molecules on either side of the mid-plane (Figures 1c, 1d) and for the positional
222 distribution of H_2O molecules derived from MC simulations incomplete. The 2WG
223 distributions considered in the present study are symmetrical relative to the interlayer mid-
224 plane. They are characterized by the distance (Δd) between this mid-plane, where interlayer
225 cations are supposed to be located, and the position of the maximum density of the Gaussian
226 distribution. In addition, the total amount of interlayer H_2O molecules was refined together
227 with the full width at half maximum intensity (FWHM) parameter of the Gaussian
228 distribution. In the resulting structure model, H_2O molecules were introduced using a 0.05 Å
229 step along the c* axis, with a B_{wat} factor equal to zero, as thermal motion is taken into account
230 in MC calculations.

231 Two parameters were used to assess the overall goodness of fit. The unweighted R_p
232 parameter was considered because this parameter is mainly influenced by the most intense
233 diffraction maxima such as the 001 reflection which contains essential information on the
234 proportions of the different layer types and on their respective layer thickness values. The R_{wp}
235 parameter was also used to better account for the overall fit quality, especially in the high-
236 angle regions.[38] Accessory quartz reflections were omitted for the calculation of these
237 parameters. On their low-angle side, calculated XRD patterns are limited to ~5°2θ CuKα
238 because significant discrepancies, possibly resulting from an incorrect description of
239 crystalline defects not challenging the results described in the present study,[18] are observed
240 over the low-angle region.[39]

241 **Monte-Carlo simulations**. Monte-Carlo simulations in the NVT ensemble were used
242 to obtain a detailed spatial distribution of the different species within smectite interlayers. The
243 model montmorillonite-type smectite used in the simulations has a

$Na_{0.75}(Si_8)(Al_{3.25}Mg_{0.75})O_{20}(OH)_4$ structural formula and exhibits substitutions only in the octahedral sheet. The simulation box includes two 2:1 layers, each consisting of 8 unit cells (total area: 20.72 Å × 17.94 Å, thickness of the 2:1 layer: 6.54 Å). The total negative charge of the 2:1 layers was thus compensated for by 6 Na^+ cations in the interlayer. The interlayer shift between adjacent 2:1 layers was set to different arbitrary values for the two interlayers considered and not allowed to vary during the calculation. For the typical layer thickness value (15.52 Å) determined for Na-montmorillonite by XRD profile modeling, the water content was estimated from the results of previous MC simulations performed with the NPT ensemble. Series of such simulations allows the determination of layer thickness as a function of water content, at constant pressure and temperature,[40] and the water content was found to be 9.5 H_2O molecules per $O_{20}(OH)_4$. The resulting distributions of H_2O molecules within 2W smectite interlayers were collected over 5 million MC steps, normalized and made symmetric with respect to the mid-plane of the interlayer. The 2:1 layers were considered as rigid, and modeled with the rigid SPC/E model (O-H bond 1.0 Å, angle H-O-H 109.47°, charges -0.848 e^- and +0.424 e^- for oxygen and hydrogen atoms, respectively). Applied interaction potentials were the Lennard-Jones 6-12 and Coulombic potentials. Each atom in the simulation cell was thus characterized by two Van der Waals parameters and by its charge. Additional details on the MC simulations can be found elsewhere.[25,41-43] Density profiles determined from MC calculations for interlayer sodium and H_2O molecules were introduced in the XRD profile calculation using a 0.075 Å step.

Results

Influence of the Gaussian distribution profile on the relative intensity of 00ℓ reflections. Figure 2 illustrates the influence of the different parameters used to describe the

Gaussian distribution of H_2O molecules, that is the total amount of H_2O molecules (nH_2O), Δd, and FWHM, on the relative intensity of 00ℓ reflections. Calculations were performed assuming a periodic Ca-SWy-1 2W structure (layer thickness = 15.2 Å), and calculated intensities were systematically normalized to that of the 001 reflection. By increasing the total amount of H_2O molecules the intensity of the 002, 003, 005 reflections greatly increases, that of the 008 reflection also increases but to a lower extent whereas 004, 006 and 007 reflections are essentially unaffected (Figure 2). As its influence on 007 and 008 reflection intensity is limited, the nH_2O parameter will not affect significantly the intensity ratio between these two reflections which is a common and critical discrepancy between experimental and calculated profiles (Figures 1a-d). On the contrary, the 008:007 intensity ratio is strongly affected by the FWHM of the Gaussian distribution, this ratio being minimum for a Dirac distribution and increasing with the FWHM of the distribution. The 007 reflection is actually more intense than the 008 one for FWHM values larger than ~1.3 Å (Figure 2). In addition this parameter may be strongly constrained from its major influence on the intensity ratio between two intense reflections (003 and 005 reflections) which can be reversed by increasing the width of the Gaussian distribution of H_2O molecules. However, the 003:005 ratio is also affected by the Δd parameter which also affects the 008:007 intensity ratio, both ratios increasing with increasing Δd values. By increasing either the Δd parameter or the FWHM, the intensity of the 002 reflection is systematically decreased, whereas that of the 004 reflection is increased or decreased, respectively. The intensity calculated for the 006 reflection is low whatever the values used for these two parameters.

Modeling of XRD patterns. For all XRD patterns recorded on smectite samples, calculations were performed using three different configurations of H_2O molecules in the interlayers of 2W layers: (i) a 2WS configuration with two planes of H_2O molecules characterized by a B_{wat} factor of 2 $Å^2$ and a Δd parameter of 1.2 Å,[18] (ii) a similar 2WS

294 configuration with a larger Debye-Waller factor (B_{wat} = 11 Å^2), and (iii) a configuration with
295 H_2O molecules distributed according to the 2WG configuration. Optimum parameters used to
296 characterize smectite hydration heterogeneity, that is the relative proportions of the different
297 MLSs coexisting in the sample and their compositions (relative proportions of 2W, 1W, and
298 0W layers) are reported in Table 1 together with the layer thickness values for the different
299 layer types, N, σ^*, σ_z and the water content in 1W layers. For 2W layers, the water content,
300 the Δd parameter, and the FWHM of the Gaussian distribution are reported in Table 2 for the
301 different configurations of interlayer H_2O molecules.

302 *Ca-saturated montmorillonite*. For sample Ca-SWy-1 at 80% RH, the calculations
303 performed for 2WS configurations of H_2O molecules (Δd = 1.2 Å) and B_{wat} factors of 2 and
304 11 Å^2 have been described above (Figures 1c, 1d). The 2WS configuration provides a
305 satisfactory fit to experimental patterns for 00ℓ reflections with ℓ<6. However, this model
306 does not allow concealing the discrepancy observed over the high-angle range, and more
307 especially for the 008:007 intensity ratio, even if the Debye-Waller factor of H_2O molecules is
308 maximized (B_{wat} = 10-11 Å^2).[44] In this case, the water content and the Δd parameter are
309 increased from 6.6 to 6.8 H_2O per $O_{20}(OH)_4$ and from 1.20 to 1.32 Å, respectively, as
310 compared to the 2WS configuration with B_{wat} = 2 Å^2 (Table 2). A 008:007 intensity ratio
311 consistent with that observed experimentally can be obtained by considering the 2WG
312 configuration for interlayer H_2O molecules. In this case, broad Gaussian distributions were
313 assumed (FWHM = 1.7 Å), and both the water content and the Δd parameter were increased
314 as compared to alternative interlayer configurations (Table 2). This 2WG configuration also
315 allows fitting better the profile of the 005 reflection, but that of the 003 one is slightly altered
316 as a result of a low-angle tail broadening (Figure 1e).

317 The combination of two structures, a main periodic one with only 2W layers and a
318 second one containing the three layer types (Table 1), accounts for the hydration

heterogeneity of sample Ca-SWy-2 at 40% RH, and leads to the coexistence of 2W, 1W, and 0W layers (95%, 4%, and 1%, respectively).[20] The 2WS configuration allows describing most features of the experimental XRD patterns (R_p = 1.31% and R_{wp} = 8.13% – Figure 3a). However, the 008 reflection is significantly more intense than the 007 one. By increasing the Debye-Waller B_{wat} factor from 2 to 11 Å^2, the 008:007 intensity ratio appears closer to the experimental one although the two estimates of the fit quality are not affected (Figure 3b). This ratio is best reproduced by assuming a 2WG distribution with a FWHM of 1.4 Å (Figure 3c) although R_p and R_{wp} parameters are almost unaffected. As compared to the 2WS mode, the total amount of H_2O molecules in such 2WG configuration is considerably increased from 6.2 (assuming a B_{wat} factor of 2 Å^2) to 7.8 per $O_{20}(OH)_4$ (Table 2).

Sr-saturated montmorillonite. At both 60 and 80% RH, the hydration heterogeneity of sample Sr-SWy-1 is minimum as it contains an overwhelming proportion of 2W layers (95, and 96%, respectively – Table 1).[18] As for the Ca-saturated samples, the 2WS configuration for H_2O molecules leads to a satisfactory fit to the experimental XRD patterns, especially for 00ℓ reflections with ℓ<6, and for the 008 reflection (Figures 4a, 5a). However, significant discrepancies between experimental and calculated patterns are visible for the 002 reflection and the 008:007 intensity ratio. These discrepancies are significantly reduced by increasing the Debye-Waller factor of H_2O molecules from 2 to 11 Å^2, but they do not vanish completely (Figures 4b, 5b). The optimum fit to the experimental XRD patterns was again obtained assuming a 2WG distribution of interlayer H_2O molecules with a large FWHM value (1.2, and 1.5 Å for Sr-SWy-1 samples recorded at 60 and 80% RH, respectively – Table 2; Figures 4c, 5c). For the two samples, both Rp and Rwp are lower for the 2WG configuration of interlayer H_2O molecules than for the 2WS ones.

Na-saturated montmorillonite. At 80% RH, the Na-SWy-2 sample exhibits a high proportion (92%) of 2W layers whereas minor amounts of 1W and 0W layers (5%, and 3%,

344 respectively) account for the hydration heterogeneity (Table 1). As for the previous sample,
345 the 2WS configuration of H_2O molecules leads to a satisfactory agreement between
346 experimental and calculated data, especially for 00ℓ reflections with ℓ<6, and for the 008
347 reflection (Figure 6a). However, by using a Debye-Waller factor of 2 $Å^2$ the intensity
348 calculated for the 006 and 007 reflections are too low as compared to the experimental one.
349 Increasing the B_{wat} factor up to 11 $Å^2$ significantly reduces these discrepancies although the
350 008:007 intensity ratio remains imperfectly reproduced (Figure 6b). The optimum fit to the
351 experimental data for this sample was again obtained assuming a 2WG distribution of H_2O
352 molecules (Figure 6c – R_{wp} = 5.33%, R_p = 2.59%). The Δd and FWHM parameters of this
353 2WG distribution are 1.50 Å and 1.4 Å, respectively (Table 2). A similar fit to the
354 experimental data (Figure 6d – R_{wp} = 5.34%, R_p = 2.57%) was obtained assuming the
355 distribution of interlayer species shown on Figure 7, while all other parameters were kept
356 constant (Table 1). This distribution was derived from the MC simulations performed using
357 the NVT ensemble. MC calculated distributions exhibit a single peak for the oxygen atoms,
358 and two for the hydrogen atoms, between the interlayer mid-plane and the surface of the 2:1
359 layer, and are characteristic of the presence of a single plane of H_2O molecules on either side
360 of the cation plane which is located in the center of the interlayer. The distance between the
361 maximum of the oxygen distribution and the maximum of the hydrogen distribution closer to
362 the 2:1 layer is ~1.0 Å which is the length of the O-H bond in the water molecule. This
363 indicates a preferential orientation of the H_2O molecules in the interlayer, with one of the O-H
364 bonds almost perpendicular to the surface of the 2:1 layer. Similar configurations of H_2O
365 molecules in the interlayer of octahedrally-substituted smectites have been previously
366 reported from IR spectroscopy results,[45] and from microscopic simulations.[24] As for all other
367 samples, the amount of interlayer H_2O molecules has to be increased, together with the Δd
368 parameter, as the positional distribution of these species increases (Table 2).

Na-saturated synthetic saponites. At 90% RH, the hydration heterogeneity of both synthetic saponites is minimum as they exhibit an overwhelming proportion of 2W layers (94, and 97% for Na-$Sap_{0.8}$ and Na-$Sap_{1.4}$ samples, respectively – Table 1). As compared to the natural ones, these two synthetic samples present larger CSDS along the c* axis, as evidenced by the sharpening of the 00ℓ reflections (Table 1 – Figures 8, 9). Layer thickness of 2W layers decreases from 15.4 Å to 15.0 Å as the layer charge increases from 0.8 to 1.4 per $O_{20}(OH)_4$ (samples Na-$Sap_{0.8}$ and Na-$Sap_{1.4}$, respectively – Table 1). For both samples, the 2WS configuration of H_2O molecules with B_{wat} = 2 $Å^2$ allows fitting satisfactorily 00ℓ reflections with ℓ<6 (Figures 8a, 9a). Increasing the Debye-Waller factor up to 11 $Å^2$ leads to a perfect fit to the experimental data for the high-charge sample (Na-$Sap_{1.4}$ – Figure 9b),whereas significant discrepancies are still observed between experimental and calculated patterns for the low-charge sample (Na-$Sap_{0.8}$ - Figure 8b). For this latter sample, the optimum fit to the experimental data was again obtained assuming a 2WG distribution of H_2O molecules in the smectite interlayer with Δd and FWHM parameters (1.39 Å and 1.4 Å, respectively) similar to those obtained for natural samples (Figure 8c – Table 2). For the Na-$Sap_{1.4}$ sample, a fit similar to the one obtained with a 2WS distribution of H_2O molecules and a high B_{wat} factor was obtained assuming a 2WG distribution of H_2O molecules (Figures 9b, 9c). However, the FWHM parameter of this distribution is significantly lower (0.8 Å) than those typically obtained for natural samples (1.2-1.7 Å – Table 2).

Discussion

Shortcomings of the usual description of H_2O molecule positional disorder in 2W smectite interlayers. By accounting for smectite hydration heterogeneity, it is possible to model experimental XRD patterns thus gaining additional insights into the structure of

smectite interlayers. It should be noted first that the initial assumption of identical properties for all layers exhibiting the same hydration state and present in the different MLSs was verified for all samples, thus validating the proposed description of smectite hydration heterogeneity. In addition, the configuration of H_2O molecules within 2W smectite layers commonly used for XRD pattern simulations can be discarded as it systematically leads to major discrepancies between experimental and calculated profiles (Figure 10).[18-20] Specifically, the use of this usual configuration systematically leads to poor fits to the experimental XRD patterns for low-angle high-intensity reflections such as 003, 004, and 005 reflections (Figure 10). By contrast, the distribution of H_2O molecules within a single plane on either side of the mid-plane interlayer (2WS configuration) allows both fitting the profiles and reproducing the relative intensities of the 00ℓ reflections with ℓ<6 (Figures 1c, 3a, 4a, 5a, 6a, 8a, 9a).[18] When assuming a Debye-Waller B_{wat} factor of 2 $Å^2$, this model leads to significant discrepancies for high-order 00ℓ reflections, which are partly resolved by increasing the positional disorder of H_2O molecules (B_{wat} = 11 $Å^2$ – Figures 1d, 3b, 4b, 5b, 6b, 8b, 9b). However, except for sample Na-$Sap_{1.4}$, such an increased B_{wat} factor does not allow fitting satisfactorily the high-order 00ℓ reflections, which would require unrealistically high B_{wat} factor values. In addition, the contrasting B_{wat} factors adjusted for the two synthetic saponite samples recorded under similar RH conditions plead for a different origin to the actual positional disorder of H_2O molecules in smectite interlayers.

Distribution of H_2O molecules according to a double Gaussian function. The 2WG model can be considered as an improved version of the 2WS model in which the actual positional disorder of H_2O molecules is better accounted for (Figures 1e, 3c, 4c, 5c, 6c, 8c, 9c). In the 2WG model the interlayer cation is considered to lie in a fixed position located in the interlayer mid-plane and to have a Debye-Waller factor of 2 $Å^2$. This hypothesis does not imply that the interlayer cations are not distributed as H_2O molecules are, but it was assumed

419 as a first approximation that thermal motion would be sufficient to account for their positional
420 disorder In addition, the sensitivity to the positional disorder of these cations is much reduced
421 as compared to H_2O molecules as the former species accounts for a minor part of the overall
422 electronic density in smectite interlayers. For example, at 80% RH Ca^{2+} cations account for
423 only 6% of the interlayer electrons (Table 3).

424 When comparing the electronic density due to interlayer H_2O molecules deduced from
425 MC calculations with that obtained from XRD profile fitting (Figure 11a), it is possible to
426 note that the overall profiles are globally alike in spite of significant differences. In particular
427 the two planes of H_2O molecules on either side of the interlayer mid-plane are much narrower
428 in the MC calculations (FWHM ~ 0.7 Å as compared to ~1.4 Å for XRD profile fitting) which
429 indicate also a significantly higher electron density in the interlayer mid-plane. The narrower
430 distribution obtained from the MC simulation can be due in part to the fixed interlayer
431 displacement between adjacent layers considered for the calculations although the influence
432 of interlayer shift and/or layer rotation on the distribution of interlayer species derived from
433 MC simulations is expected to be limited. The simple (simplistic ?) Gaussian functions used
434 to model the distribution of H_2O molecules are both shifted toward the interlayer mid-plane
435 (by about 0.2 Å) and broadened as compared to MC calculations. Both the broadening and the
436 shift of the Gaussian distributions are likely related to the specific profile of the MC
437 distribution, and more especially to the high electron density in the interlayer mid-plane
438 (Figure 7). However, the XRD profiles calculated assuming the two models are almost
439 identical (Figures 6c, 6d), pleading for a limited sensitivity of calculated XRD patterns to
440 these two parameters if the actual distribution profile is unknown.

441 *Validity of the 2WG configuration model*. Similar XRD patterns may be calculated
442 with 2WG and 2WS models by increasing the B_{wat} factor in the latter model (Figures 8c, 8d,
443 and 9b, 9c). Because of the demonstrated sensitivity of calculated XRD patterns to the

distribution of H_2O molecules, this similarity can only result from similar contributions of H_2O molecules to the structure factor in both models. Factors affecting the structure factor include the scattering power, the position and the amount of considered species. If the origin of the layer unit is set in the center of the layer octahedron, the contribution of H_2O molecules to the structure factor of 00ℓ reflections for a periodic 2W smectite (2WS model) can be expressed as:

$$F_{H_2O}(00\ell) = 2 n_{H_2O} f_B(\frac{\sin\theta}{\lambda})_{00\ell} \cos(2\pi\ell Z) \quad (1)$$

where $f_B(\frac{\sin\theta}{\lambda})_{00\ell}$ is the scattering power of H_2O molecules taking into account their thermal motion (B_{wat}), n_{H_2O} is the amount of H_2O molecules at $Z = \frac{1}{2} - \frac{\Delta d}{h}$, h being the layer thickness. Δd is the distance between the interlayer mid-plane and the positions of the H_2O molecules along the c* axis. With increasing values of ℓ, the contribution of H_2O molecules decreases together with $f_B(00\ell)$ as a result of the thermal motion of H_2O molecules.

For the 2WG model, the contribution of interlayer H_2O molecules to the structure factor of 00ℓ reflections for a periodic 2W smectite can be expressed as:

$$F_{H_2O}(00\ell) = 4 f(\frac{\sin\theta}{\lambda})_{00\ell} \cos(2\pi\ell(\frac{1}{2} - \frac{\Delta d}{h}))\sum_m n_m \cos(2\pi\ell m\frac{\Delta z}{h}) \quad (2)$$

where $f(\frac{\sin\theta}{\lambda})_{00\ell}$ is the scattering power of H_2O molecules ($B_{wat} = 0$), and Δd is the distance along the c* axis between the interlayer mid-plane and the position of the maximum density of the Gaussian distribution. n_m is the amount of H_2O molecules at a given distance (mΔz, m being integer) from the maximum density of the Gaussian distribution. The sum $\sum_m n_m$ equals the total number of interlayer H_2O molecules. For a given ℓ value, the

positional distribution of H_2O molecules disturbs their coherent scattering and thus decreases their absolute contribution to the structure factor. The decrease becomes more important as the ℓ indice increases. To quantify this decrease, Equation (2) can be expressed as:

$$F_{H_2O}(00\ell) = 2 n_{H_2O}^{eff} f\left(\frac{\sin\theta}{\lambda}\right)_{00\ell} \cos\left(2\pi\ell\left(\frac{1}{2} - \frac{\Delta d}{h}\right)\right)\sum_m n_m \cos\left(2\pi\ell m \frac{\Delta Z}{h}\right) \quad (3)$$

where $n_{H_2O}^{eff} = 2\sum_m n_m \cos\left(2\pi\ell m \frac{\Delta Z}{h}\right)$ is the effective amount of interlayer H_2O molecules contributing to the structure factor. Equations (1) and (3) look similar but in the sum determining the $n_{H_2O}^{eff}$ value, the cosine term is lower than 1, and $n_{H_2O}^{eff}$ is thus lower than the total number of H_2O molecules. In addition, the $n_{H_2O}^{eff}$ value decreases with increasing ℓ indices.

Thus both 2WS and 2WG models are essentially different although in both cases the contribution of interlayer H_2O molecules to the structure factor is strongly decreasing with increasing ℓ indices. In the first case, the thermal motion of these interlayer species is entirely responsible for the decrease whereas in the latter model the decrease is related to the decreasing effective number of H_2O molecules contributing to coherent diffraction effects. Note that both models may produce similar diffraction effects if appropriate values are used for the parameters describing the positional disorder of interlayer molecules. However, unrealistically large values were obtained for the B_{wat} parameter when fitting Na-$Sap_{0.8}$ (B_{wat} = 30 Å^2) as compared to Na-$Sap_{1.4}$ (B_{wat} = 11 Å^2) although both XRD patterns were recorded under similar experimental conditions, and the 2WG configuration of H_2O molecules appears as more realistic than the 2WS one. Additional support for the 2WG model arises from the close match between the number of interlayer H_2O molecules determined using the 2WG model and that measured independently from water vapor isotherms.

Water content in smectite interlayer. For a given sample, the total amount of interlayer H_2O molecules can be approximated by weighing the water content hypothesized for each layer type by the relative abundance of this layer type and compared to that obtained from water vapor adsorption-desorption isotherm experiments (Table 3).[18] The water content determined by Ferrage et al. from XRD profile modeling assuming a 2WS model for the distribution of interlayer H_2O molecules was reasonably consistent with that obtained from water vapor adsorption-desorption isotherm experiments.[14,16,18] However, the 2WG configuration provides the best agreement with the water contents determined experimentally from water vapor adsorption-desorption isotherm experiments, the XRD values lying most often between the values obtained on either branches of the isotherm (Tables 2, 3).

FWHM of H_2O molecule Gaussian distribution. When using the 2WG model to describe the distribution of H_2O molecules in 2W layers, the FWHM parameter represents the positional disorder of the species, which is characterized by the B_{wat} factor in usual models. One may note that the diffraction effects resulting from the two configurations are similar and lead to a significant decrease of the coherent scattering of H_2O molecules with increasing diffraction angle (see above). However, the B_{wat} factor should be about constant for a given species whereas the FWHM parameter can be structurally interpreted. For example, when increasing the RH, the FWHM of the Gaussian distribution systematically increases for Ca- and Sr-saturated montmorillonites (Table 2 – Figures 11b, 11c) most likely to accommodate the steady addition of H_2O molecules weakly bound to the interlayer cation. On the contrary, with increasing layer charge, Na-saturated saponite samples hold more H_2O molecules for a given RH value in a narrower distribution (Figure 11d – Table 2). A possible origin for such narrowing of H_2O molecule distributions is the increased polarization of these interlayer species resulting from a stronger undersaturation of surface oxygen atoms.

511 *Relative positions of interlayer cations and H_2O molecules.* The distance (Δd) between
512 the interlayer cations, which are located in the interlayer mid-plane, and the maximum density
513 of the interlayer H_2O molecule distribution function was also varied from one model to the
514 other, the maximum Δd values being obtained with the 2WG configuration of H_2O molecules
515 (Table 2). The Δd values reported in the present study represent only indicative values that
516 could be used for XRD profile modeling but a more complete study should be carried out to
517 determine the key factors that influence this parameter.

518 **Consistency with reported interlayer structures of expandable 2:1 phyllosilicates.**

519 *Comparison with the present data*. Among expandable 2:1 phyllosilicates, vermiculite
520 and smectite are differentiated from their contrasting layer charge, vermiculite exhibiting a
521 higher layer charge (1.2-1.8 per $O_{20}(OH)_4$) than smectite (0.4-1.2 per $O_{20}(OH)_4$).[46] This
522 difference is usually revealed by the contrasting swelling behavior of the two minerals after
523 magnesium saturation and glycerol solvation, vermiculite and smectite exhibiting basal
524 spacings of ~14 Å and ~18 Å, respectively, after such treatment.[1,47,48] However, distinct
525 hydration behavior has not been reported for these two mineral species, and the predominance
526 of bi-hydrated layers has been documented for the two species as a function of relative
527 humidity. As a consequence, these two expandable 2:1 phyllosilicates will be considered
528 together in the following.

529 For modeling XRD results of clay minerals containing 2W layers, the interlayer water
530 configuration usually assumed for bi-hydrated smectite is that used for the calculations
531 showed on Figures 1a and 10 and already described (Type I – Figure 12).[1] This model does
532 not allow the description of experimental XRD patterns (Figure 10) and may be rejected.

533 Most of the three-dimensional structural determinations of 2W interlayer
534 configuration were actually performed on vermiculite as this mineral frequently exhibits
535 ordered stacking sequences and because its higher content of interlayer cations allows for a

more accurate refinement of cation positions as compared to smectite. In addition vermiculite, as illite, presents an ordered distribution of interlayer cations which eases the structural characterization of the interlayer configuration as compared to smectite.[49] The structural studies devoted to the configuration of interlayer species have led to different structure models that will be described below.

In bi-hydrated Mg-vermiculite, Mg^{2+} cations are located in the mid-plane of the interlayer with one sheet of H_2O molecules on each side of this plane (Type II - Figure 12).[5,50,51,52,53] According to this model, Mg is octahedrally coordinated by six H_2O molecules whereas additional H_2O molecules, which are weakly bound to the cation, are located on the same plane as the six cation-bound H_2O molecules.[54-57] A Type II configuration of H_2O molecules was also proposed for Na-saturated vermiculite,[58,59] and for Na-, Ca- and Li-rich altered phlogopites.[60]

A second configuration of interlayer species has been proposed for Ca-saturated vermiculites (Type III – Figure 12).[58,61,62] In this model, two distinct coordinations are reported for Ca^{2+} cations, two out of three Ca^{2+} cations being octahedrally coordinated as in type II configuration, whereas remaining Ca^{2+} cations exhibit a cubic coordination. This dual coordination induces the presence of two discrete planes of H_2O molecules (planes 2 and 3 – Figure 12) in addition to that observed in the type II configuration, which holds most H_2O molecules (plane 1 – Figure 12). The increased heterogeneity of H_2O configuration in Ca-, Sr-, and Ba-saturated samples as compared to Mg-saturated ones was confirmed both from diffraction and IR results.[56,57] A Type III configuration of H_2O molecules was also proposed for Na-saturated vermiculite.[58] Figure 13 compares the 2WG configuration of interlayer H_2O molecules determined for Ca-SWy-2 (40% RH) in the present study with that reported in the literature for Ca-saturated vermiculite.[58,61] After normalization of the three distributions to the denser plane of H_2O molecules, the three planes of H_2O molecules appear closely related to

561 the 2WG configuration proposed in the present study to describe the positional distribution of
562 interlayer species.

563 To compare the Δd values obtained in the present study with those reported in the
564 literature (1.14-1.45 Å – Table 4), these values can be normalized to the thickness of the
565 interlayer space to account better for the balance of the interactions with the interlayer cation
566 on the one hand and the 2:1 layer on the other hand (Table 5). Following such a normalization
567 procedure, the Δd values determined for the 2WG configuration of H_2O molecules are
568 consistent with those reported in the literature whereas lower values are obtained when
569 assuming a 2WS configuration.

570 In addition, z-coordinates along c* axis were recalculated together with typical
571 distances between the 2:1 layer and the planes of H_2O molecules, and between H_2O molecules
572 and interlayer cations (Table 4). For type II and III configurations the distance between the
573 2:1 layer and the densest plane of H_2O molecules scatters between 2.36 Å and 2.82 Å and is
574 consistent with the formation of H-bonds between interlayer H_2O molecules and the clay
575 framework. The distance between the densest plane of H_2O molecules and the interlayer
576 cation ranges from 1.14-1.45 Å.

577 *Specific interlayer structure resulting from the presence of tetrahedral substitutions.* A
578 third configuration of water in 2W smectite has been envisaged for Na-beidellite samples,
579 with Na^+ cations being partly engaged in the ditrigonal cavities of the 2:1 layers and the
580 coordinated H_2O molecules distributed on either side of the interlayer mid-plane which is
581 devoid of atoms (Type IV – Figure 12).[12,13,63] Such a migration of the interlayer cation from
582 the interlayer mid-plane toward the 2:1 clay framework is consistent with MC simulations and
583 IR spectroscopy results which both support the formation of inner-sphere complexes for
584 monovalent cations in tetrahedrally substituted 2:1 phyllosilicates.[21,24,26,31] In the present
585 study, similar distributions of interlayer species have been determined whatever the location

586 of the layer charge deficit in agreement with previous reports of Type II and Type III
587 configurations of interlayer species in tetrahedrally substituted 2W vermiculites.[58-60] The
588 central location of Na^+ cations was found to be consistent with experimental XRD data even
589 when Na^+ cations account for a significant part of the interlayer electronic density (13% of the
590 interlayer electrons for sample Na-$Sap_{1.4}$). Furthermore, if a Type IV configuration is assumed
591 for the distribution of interlayer species, significant discrepancies arise between experimental
592 and calculated patterns, especially for the 002 and 003 reflections which are extremely
593 sensitive to the presence of interlayer species at the interlayer mid-plane position (Figure 14).
594 In conclusion, the present data does not provide experimental evidence for the migration of
595 monovalent cations toward the surface of tetrahedrally substituted 2:1 layers.
596

597 **Acknowledgments**

598 The results presented are a part of a Ph.D. thesis granted by Andra (French National
599 Agency for Nuclear Waste Disposal). Andra is thanked for the permission to publish this
600 manuscript and for financial support. BL acknowledges financial support from the
601 CNRS/PICS709 program, and from the CNRS/SdU “postes rouges” fellowships granted to
602 BAS. VAD and BAS are grateful to the Russian Science Foundation for partial financial
603 support. Laurent Michot (LEM, Nancy – France) is thanked for the fruitful discussions about
604 smectite hydration. Jean-Louis Robert (IST Orléans, France) kindly provided the synthetic
605 saponite samples.
606

607 **Literature cited**

608

(1) Moore, D. M.; Reynolds, R. C., Jr *X-ray Diffraction and the Identification and Analysis of Clay Minerals*; Oxford University Press: Oxford and New York, 1997.

(2) Nagelschmidt, G. *Z. Kristallogr.* **1936**, *93*, 481-487.

(3) Bradley, W. F.; Grim, R. E.; Clark, G. F. *Z. Kristallogr.* **1937**, *97*, 260-270.

(4) Mooney, R. W.; Keenan, A. G.; Wood, L. A. *J. Am. Chem. Soc.* **1952**, *74*, 1371-1374.

(5) Walker, G. F. *Clays & Clay Miner.* **1956**, *4*, 101-115.

(6) Norrish, K. *Discuss. Faraday Soc.* **1954**, *18*, 120-133.

(7) Van Olphen, H. *J. Colloid Sci.* **1965**, *20*, 822-837.

(8) Kittrick, J. A. *Soil Sci. Soc. Am. J.* **1969a**, *33*, 217-222.

(9) Kittrick, J. A. *Soil Sci. Soc. Am. J.* **1969b**, *33*, 222-225.

(10) Laird, D. A. *Clays & Clay Miner.* **1996**, *44*, 553-559.

(11) Laird, D. A. *Clays & Clay Miner.* **1999**, *47*, 630-636.

(12) Ben Brahim, J.; Besson, G.; Tchoubar, C. In *5th Meeting of the European Clay Groups*: Prague, 1983, pp 65-75.

(13) Ben Brahim, J.; Besson, G.; Tchoubar, C. *J. Appl. Cryst.* **1984**, *17*, 179-188.

(14) Bérend, I.; Cases, J. M.; François, M.; Uriot, J. P.; Michot, L. J.; Masion, A.; Thomas, F. *Clays & Clay Miner.* **1995**, *43*, 324-336.

(15) Cases, J. M.; Bérend, I.; Besson, G.; François, M.; Uriot, J. P.; Thomas, F.; Poirier, J. P. *Langmuir* **1992**, *8*, 2730-2739.

(16) Cases, J. M.; Bérend, I.; François, M.; Uriot, J. P.; Michot, L. J.; Thomas, F. *Clays & Clay Miner.* **1997**, *45*, 8-22.

(17) Cuadros, J. *Amer. J. Sci.* **1997**, *297*, 829-841.

(18) Ferrage, E.; Lanson, B.; Sakharov, B. A.; Drits, V. A. *Amer. Mineral.* **2005**, in press Ms #1776R.

(19) Ferrage, E.; Lanson, B.; Sakharov, B. A.; Geoffroy, N.; Drits, V. A. *Amer. Mineral.* **2005**, in preparation.

(20) Ferrage, E.; Tournassat, C.; Rinnert, E.; Lanson, B. *Geochim. Cosmochim. Acta* **2005**, in press Ms #2963.

(21) Skipper, N. T.; Chang, F. R. C.; Sposito, G. *Clays & Clay Miner.* **1995**, *43*, 285-293.

(22) Chang, F. R. C.; Skipper, N. T.; Sposito, G. *Langmuir* **1998**, *14*, 1201-1207.

(23) Boek, E. S.; Coveney, P. V.; Skipper, N. T. *J. Am. Chem. Soc.* **1995**, *117*, 12608-12617.

(24) Chang, F. R. C.; Skipper, N. T.; Sposito, G. *Langmuir* **1995**, *11*, 2734-2741.

(25) Chang, F. R. C.; Skipper, N. T.; Sposito, G. *Langmuir* **1997**, *13*, 2074-2082.

(26) Skipper, N. T.; Sposito, G.; Chang, F. R. C. *Clays & Clay Miner.* **1995**, *43*, 294-303.

(27) Skipper, N. T.; Refson, K.; McConnell, J. D. C. *J. Chem. Phys.* **1991**, *94*, 7434-7445.

(28) Greathouse, J.; Refson, K.; Sposito, G. *J. Am. Chem. Soc.* **2000**, *122*, 11459-11464.

(29) Sposito, G.; Skipper, N. T.; Sutton, R.; Park, S. H.; Soper, A. K.; Greathouse, J. A. *Proc. Nat. Acad. Sci. USA* **1999**, *96*, 3358-3364.

(30) Michot, L. J.; Villiéras, F. *Clay Miner.* **2002**, *37*, 39-57.

(31) Pelletier, M.; Michot, L. J.; Humbert, B.; Barres, O.; D'espinose de la Callerie, J. B.; Robert, J. L. *Amer. Mineral.* **2003**, *88*, 1801-1808.

(32) Drits, V. A.; Sakharov, B. A. *X-Ray structure analysis of mixed-layer minerals*; Dokl. Akad. Nauk SSSR: Moscow, 1976.

(33) Drits, V. A.; Lindgreen, H.; Sakharov, B. A.; Salyn, A. S. *Clay Miner.* **1997**, *33*, 351-371.

(34) Sakharov, B. A.; Lindgreen, H.; Salyn, A.; Drits, V. A. *Clays & Clay Miner.* **1999**, *47*, 555-566.

(35) Drits, V. A.; Srodon, J.; Eberl, D. D. *Clays & Clay Miner.* **1997**, *45*, 461-475.

(36) Guinier, A. *Théorie et technique de la radiocristallographie*; Dunod: Paris, 1964.

(37) Drits, V. A.; Tchoubar, C. *X-ray diffraction by disordered lamellar structures: Theory and applications to microdivided silicates and carbons*; Springer-Verlag: Berlin, 1990.

(38) Howard, S. A.; Preston, K. D. In *Modern Powder Diffraction*; Bish, D. L., Post, J. E., Eds.; Mineralogical Society of America: Wahington D.C., 1989; Reviews in Mineralogy Vol. 20, pp 217-275.

(39) Plançon, A. *Amer. Mineral.* **2002**, *87*, 1672-1677.

(40) Marry, V., *Ph.D. dissertation*, Pierre et Marie Curie University - Paris, 2002.

(41) Marry, V.; Turq, P.; Cartailler, T.; Levesque, D. *J. Chem. Phys.* **2002**, *117*, 3454-3463.

(42) Delville, A. *Langmuir* **1992**, *8*, 1796-1805.

(43) Boek, E. S.; Coveney, P. V. ; Skipper, N. T. *Langmuir* **1995**, *11*, 4629-4631.

(44) Lipson, H. In *International tables for X-ray crystallography*;; Casper, J. S., Lonsdale, K., Eds., 1967; International Union of Crystallography; Mathematical tables Vol. 2 - Mathematical tables, pp 235-315.

(45) Sposito, G.; Prost, R. *Chem. Rev.* **1982**, *82*, 553-573.

(46) Bailey, S. W. *Clay Miner.* **1980**, *15*, 85-93.

(47) Calle, C. de la; Suquet, H. In *Hydrous Phyllosilicates (exclusive of micas)*; Bailey, S. W., Ed.; Mineralogical Society of America: Washington, D.C., 1988; Reviews in Mineralogy Vol. 19, pp 455-496.

(48) Walker, G. F. *Clay Miner. Bull.* **1958**, *3*, 302-313.

(49) Besson, G.; Misfud, A.; Tchoubar, C.; Méring, J. *Clays & Clay Miner.* **1974**, *22*, 379-384.

(50) Mathieson, A. M.; Walker, G. F. *Amer. Mineral.* **1954**, *39*, 231-255.

(51) Mathieson, A. M. *Amer. Mineral.* **1958**, *43*, 216-227.

(52) Bradley, W. F.; Serratosa, J. M. In *Clays & Clay Minerals, Proceeding of the 7th Clay Conference*; Pergamon Press, 1960, pp 260-270.

(53) Shirozu, H.; Bailey, S. W. *Amer. Mineral.* **1966**, *51*, 1124-1143.

(54) Alcover, J. F.; Gatineau, L.; Méring, J. *Clays & Clay Miner.* **1973**, *21*, 131-136.

(55) Alcover, J. F.; Gatineau, L. *Clay Miner.* **1980**, *15*, 25-35.

(56) Alcover, J. F.; Gatineau, L. *Clay Miner.* **1980**, *15*, 239-248.

(57) Fornés, V.; Calle, C. de la; Suquet, H.; Pezerat, H. *Clay Miner.* **1980**, *15*, 399-411.

(58) Slade, P. G.; Stone, P. A.; Radoslovitch, E. W. *Clays & Clay Miner.* **1985**, *33*, 51-61.

(59) Beyer, J.; Graf von Reichenbach, H. *Clay Miner.* **2002**, *37*, 157-168.

(60) Le Renard, J.; Mamy, J. *Bull. Groupe Franç. Argiles* **1971**, *23*, 119-127.

(61) Calle, C. de la; Pezerat, H.; Gasperin, M. *J. Phys.* **1977**, *C7*, 128-133.

(62) Calle, C. de la; Suquet, H.; Dubernat, J.; Pezerat, H. *Clay Miner.* **1978**, *13*, 275-197.

706 (63) Ben Brahim, J.; Armagan, N.; Besson, G.; Tchoubar, C. *J. Appl. Cryst.* **1983**,
707 *16*, 264-269.

Figure captions

Figure 1. Comparison between experimental and calculated XRD patterns for the Ca-saturated SWy-1 montmorillonite sample recorded at 80% RH. Structural parameters used for the calculations are listed in Tables 1, 2, and 3. Experimental data are shown as crosses whereas calculated profiles are shown as solid lines. Solid arrows indicate a significant misfit between experimental and calculated patterns, whereas gray and open arrows indicate poor and good fits, respectively. 00ℓ reflections are indexed in parentheses. (a) Calculation for a periodic bi-hydrated structure (layer thickness of 2W layers = 15.48 Å) assuming the usual configuration of H_2O molecules.[1] (b) Calculation for a periodic bi-hydrated structure (layer thickness of 2W layers: 15.48 Å) assuming a 2WS configuration (see text for details) with B_{wat} = 2 $Å^2$ for H_2O molecules.[18] (c) Calculation performed accounting for hydration heterogeneities and assuming a 2WS configuration with B_{wat} = 2 $Å^2$ for H_2O molecules.[18] Hydration heterogeneity was described by assuming the coexistence of a major MLS containing 2W and 1W layers (95:5 ratio) and of a second structure containing the three layer types (2W:1W:0W = 85:13:2) in a 61:39 ratio (Table 2). (d) Calculation performed accounting for hydration heterogeneities and assuming a 2WS configuration with B_{wat} = 11 $Å^2$ for H_2O molecules. (e) Calculation performed accounting for hydration heterogeneities and assuming a 2WG configuration (see text for details).

Figure 2. Relative intensities of 00ℓ reflections, after normalization to the 001 reflection, as a function of structural parameters specific to the 2WG configuration (see text for details). The total amount of H_2O molecules (nH_2O) is given per $O_{20}(OH)_4$, whereas the full width at half maximum intensity (FWHM) of the distribution and the distance, in projection along the c* axis, from its maximum to the interlayer mid-plane (Δd) are given in Å.

732 **Figure 3**. Comparison between experimental and calculated XRD patterns for the Ca-
733 saturated SWy-2 montmorillonite sample recorded at 40% RH. Structural parameters used for
734 the calculations are listed in Tables 1, 2, and 3. Patterns as for Figure 1. * indicates hk bands,
735 whereas vertical ticks denote the presence of accessory quartz reflections. (a) Calculation
736 performed assuming a 2WS configuration with B_{wat} = 2 Å^2 for H_2O molecules.[18] (b)
737 Calculation performed assuming a 2WS configuration with B_{wat} = 11 Å^2 for H_2O molecules.
738 (c) Calculation performed assuming a 2WG configuration.
739 **Figure 4**. Comparison between experimental and calculated XRD patterns for the Sr-saturated
740 SWy-1 montmorillonite sample recorded at 60% RH. Structural parameters used for the
741 calculations are listed in Tables 1, 2, and 3. Patterns as for Figure 1. (a) Calculation performed
742 assuming a 2WS configuration with B_{wat} = 2 Å^2 for H_2O molecules.[18] (b) Calculation
743 performed assuming a 2WS configuration with B_{wat} = 11 Å^2 for H_2O molecules. (c)
744 Calculation performed assuming a 2WG configuration.
745 **Figure 5**. Comparison between experimental and calculated XRD patterns for the Sr-saturated
746 SWy-1 montmorillonite sample recorded at 80% RH. Structural parameters used for the
747 calculations are listed in Tables 1, 2, and 3. Patterns as for Figure 1. (a) Calculation performed
748 assuming a 2WS configuration with B_{wat} = 2 Å^2 for H_2O molecules.[18] (b) Calculation
749 performed assuming a 2WS configuration with B_{wat} = 11 Å^2 for H_2O molecules. (c)
750 Calculation performed assuming a 2WG configuration.
751 **Figure 6**. Comparison between experimental and calculated XRD patterns for the Na-
752 saturated SWy-2 montmorillonite sample recorded at 80% RH. Structural parameters used for
753 the calculations are listed in Tables 1, 2, and 3. Patterns as for Figures 1 and 3. (a) Calculation
754 performed assuming a 2WS configuration with B_{wat} = 2 Å^2 for H_2O molecules.[18] (b)
755 Calculation performed assuming a 2WS configuration with B_{wat} = 11 Å^2 for H_2O molecules.
756 (c) Calculation performed assuming a 2WG configuration. (d) Calculation performed

757 assuming the distribution of interlayer species derived from MC simulations using the NVT
758 ensemble and shown in Figure 7.
759 **Figure 7**. Density profiles of interlayer species along the c* axis derived from MC
760 simulations performed using the NVT ensemble. z-coordinates are given in Å with the origin
761 located in the interlayer mid-plane. Solid, dashed and gray lines represent O, H, and Na^+
762 atoms, respectively.
763 **Figure 8**. Comparison between experimental and calculated XRD patterns for the Na-
764 saturated $Sap_{0.8}$ saponite sample recorded at 90% RH. Structural parameters used for the
765 calculations are listed in Tables 1, 2, and 3. Patterns as for Figure 1. (a) Calculation performed
766 assuming a 2WS configuration with B_{wat} = 2 $Å^2$ for H_2O molecules.[18] (b) Calculation
767 performed assuming a 2WS configuration with B_{wat} = 11 $Å^2$ for H_2O molecules. (c)
768 Calculation performed assuming a 2WG configuration. (d) Calculation performed assuming a
769 2WS configuration with B_{wat} = 30 $Å^2$ for H_2O molecules, 10.5 nH_2O molecules per $O_{20}(OH)_2$)
770 in 2W layers, and Δd =1.38 Å.
771 **Figure 9**. Comparison between experimental and calculated XRD patterns for the Na-
772 saturated $Sap_{1.4}$ saponite sample recorded at 90% RH. Structural parameters used for the
773 calculations are listed in Tables 1, 2, and 3. Patterns as for Figure 1. (a) Calculation performed
774 assuming a 2WS configuration with B_{wat} = 2 $Å^2$ for H_2O molecules.[18] (b) Calculation
775 performed assuming a 2WS configuration with B_{wat} = 11 $Å^2$ for H_2O molecules. (c)
776 Calculation performed and assuming a 2WG configuration.
777 **Figure 10**. Comparison between experimental XRD patterns and those calculated assuming
778 the usual configuration of H_2O molecules.[1] Hydration heterogeneity has been taken into
779 account for all calculations. Structural parameters used for the calculations are listed in Table
780 1. Patterns as for Figures 1 and 3. (a) Ca-saturated SWy-1 montmorillonite sample recorded at
781 80% RH. (b) Ca-saturated SWy-2 montmorillonite sample recorded at 40% RH. (c) Sr-

saturated SWy-1 montmorillonite sample recorded at 60% RH. (d) Sr-saturated SWy-1 montmorillonite sample recorded at 80% RH. (e) Na-saturated SWy-2 montmorillonite sample recorded at 80% RH. (f) Na-saturated $Sap_{0.8}$ saponite sample recorded at 90% RH. (g) Na-saturated $Sap_{1.4}$ saponite sample recorded at 90% RH.

Figure 11. Density profiles along the c* axis of the electron distribution in the interlayer of bi-hydrated smectite layers. z-coordinates are given in Å with the origin located in the interlayer mid-plane. (a) Comparison between the electron distribution derived from the density profiles of interlayer species calculated using the NVT ensemble (Figure 7) and the one determined from XRD profile modeling for the Na-SWy-2 montmorillonite sample (80% RH). (b) Comparison between the electron distributions determined from XRD profile modeling for the two Ca-saturated montmorillonite samples under different RH conditions. (c) Comparison between the electron distributions determined from XRD profile modeling for the two Sr-saturated SWy-1 montmorillonite samples under different RH conditions. (d) Comparison between the electron distributions determined from XRD profile modeling for the two Na-saturated synthetic saponite samples with different amounts of layer charge.

Figure 12. Schematic description of the different configurations proposed in the literature for interlayer species in 2W smectite layers. O and T refer to the octahedral and tetrahedral sheets of the 2:1 layer, respectively. Labels of the different sheets of H_2O molecules are detailed in the text.

Figure 13. Comparison of the distributions of H_2O molecules reported for bi-hydrated smectites. The distributions are normalized to the denser plane of H_2O molecules, and z-coordinates are given in fraction of the interlayer with the origin located in the interlayer mid-plane after normalization to the interlayer thickness. The distribution determined from XRD profile modeling for the Ca-saturated SWy-2 montmorillonite sample (40% RH) is plotted as

806 a solid line, whereas data from De la Calle et al. and from Slade et al. are shown as dashed
807 and dotted-dashed lines, respectively.[58,61]
808 **Figure 14**. Comparison between experimental and calculated XRD patterns for the Na-
809 saturated $Sap_{1.4}$ saponite sample recorded at 90% RH. Structural parameters used for the
810 calculations are listed in Tables 1, 2, and 3. Patterns as for Figure 1. Calculation is performed
811 assuming a Type IV configuration of interlayer species with a shift of the interlayer cation
812 from the interlayer mid-plane toward the 2:1 clay framework.[13]
813

Table 1. Optimum structural parameters used for the simulation of experimental XRD profiles.

Sample	Rel. ab. (%)[a]	2W[b]	1W[b]	0W[b]	L. Tck. 2W[c]	L. Tck. 1W[c]	L. Tck. 0W[c]	nH_20 1W[d]	N[e]	σ*[f]	σ_z[g]
Ca-SWy-2 (40%RH)[h]	87	100	0	0	15.18	12.60	10.00	3.2	8.7	6.5	0.35
	13	60	30	10							
Ca-SWy-1 (80%RH)[i]	61	95	5	0	15.51	12.85	10.00	3.3	6.0	6.5	0.27
	39	85	13	2							
Sr-SWy-1 (60%RH)[i]	82	100	0	0	15.53	12.58	10.00	3.5	7.5	5.5	0.35
	18	75	15	10							
Sr-SWy-1 (80%RH)[i]	84	100	0	0	15.73	12.70	10.00	5.5	7.5	5.5	0.35
	16	75	15	10							
Na-SWy-2 (80%RH)	90	96	2	2	15.52	12.55	9.60	3.2	8.2	11.0	0.25
	10	60	30	10							
$Na\text{-}Sap_{0.8}$ (90%RH)	44	100	0	0	15.40	13.20	9.80	5.7	13.0	2.0	0.19
	56	90	5	5							
$Na\text{-}Sap_{1.4}$ (90%RH)	91	100	0	0	15.00	12.90	9.80	5.0	12.0	11	0.12
	9	70	20	10							

[a] Relative proportion of the different contributions to the diffracted intensity. [b] Relative proportion of the different layer types in the different contributions to the diffracted intensity. 2W, 1W, and 0W stand for bi-hydrated, mono-hydrated and de-hydrated smectite layers, respectively. [c] Layer thickness (L. Tck.) of the different layer types. [d] Number of H_2O molecules in 1W layers (per $O_{20}(OH)_4$). [e] Mean thickness of the coherent scattering domain size along the c* axis (in layers). [f] Sigmastar parameter characterizing the sample orientation (in °).[1] [g] Standard deviation of the layer thickness parameter (in Å).[18] [h] Data from Ferrage et al.[20] [i] Data from Ferrage et al.[18]

Table 2. Structural parameters of the interlayer space determined from XRD profile modeling as a function of the assumed water configuration.

Sample	2WS, B_{wat} = 2[a]		2WS, B_{wat} = 11[a]		2WG[b]		
	nH_20[c]	Δd[d]	nH_20	Δd	nH_20	Δd	FWHM[e]
Ca-SWy-2 (40%RH)	6.2	1.20	6.6	1.30	7.8	1.34	1.4
Ca-SWy-1 (80%RH)	6.6	1.20	6.8	1.32	10.0	1.37	1.7
Sr-SWy-1 (60%RH)	6.0	1.20	6.8	1.32	8.5	1.40	1.2
Sr-SWy-1 (80%RH)	6.0	1.20	7.0	1.41	9.5	1.52	1.5
Na-SWy-2 (80%RH)	7.4	1.20	8.2	1.41	9.5	1.50	1.4
$Na\text{-}Sap_{0.8}$ (90%RH)	8.5	1.20	9.3	1.33	10.5	1.39	1.4
$Na\text{-}Sap_{1.4}$ (90%RH)	8.4	1.20	9.0	1.33	9.4	1.35	0.8

[a] 2WS corresponds to an interlayer configuration of H_2O molecules distributed as one plane on either side of the interlayer mid-plane. The Debye-Waller temperature factor for water (B_{wat}) given in $Å^2$. [b] 2WG corresponds to an interlayer configuration of H_2O molecules distributed according to a Gaussian function on either side of the interlayer mid-plane. [c] The number of H_2O molecules is given per $O_{20}(OH)_4$. In this case, B_{wat} = 0 $Å^2$. [d] The distance, in projection along the c* axis, between the interlayer mid-plane and the maximum density of the distribution of H_2O molecules (Δd) is given in Å. [e] The width of the Gaussian distribution of interlayer H_2O molecules (FWHM) is given in Å.

Table 3. Optimum amounts of H_2O molecules determined from XRD profile modeling for the different configurations of interlayer species, and from water vapor adsorption/desorption isotherms.

Sample	Type I configuration[a]	2WS $B_{wat} = 2$[b]	2WS $B_{wat} = 11$[b]	2WG[c]	Ads./Des.[d]
Ca-SWy-2 (40%RH)	7.25[e]	8.32	8.58	10.11	8.62/10.17
Ca-SWy-1 (80%RH)	7.06	8.30	8.54	12.36	12.85/13.70
Sr-SWy-1 (60%RH)	7.06	7.60	8.85	10.72	7.87/9.29 (10.70/11.90)
Sr-SWy-1 (80%RH)	7.14	7.69	8.95	12.09	9.83/10.45 (12.80/13.70)
Na-SWy-2 (80%RH)	7.04	9.27	10.24	11.82	10.50/13.10
$Na\text{-}Sap_{0.8}$ (90%RH)	7.00	10.62	11.60	13.07	13.39/14.49[f]
$Na\text{-}Sap_{1.4}$ (90%RH)	6.96	10.45	11.19	11.62	14.23/17.18[f]

[a] Interlayer configuration of H_2O molecules commonly used for the calculation XRD profiles including 2W layers.[1] [b] 2WS corresponds to an interlayer configuration of H_2O molecules distributed as one plane on either side of the interlayer mid-plane. The Debye-Waller temperature factor for water (B_{wat}) given in $Å^2$. [c] 2WG corresponds to an interlayer configuration of H_2O molecules distributed according to a Gaussian function on either side of the interlayer mid-plane. In this case, $B_{wat} = 0$ $Å^2$. [d] Water amounts determined experimentally from water vapor adsorption/desorption isotherms. Data are taken from Cases et al.,[16] and from Bérend et al.[14] for divalent and monovalent cations, respectively. [e] The water contents are given in mmol of water per g of clay. [f] Personal communication from Laurent Michot (LEM, Nancy, France).

Table 4. Structural parameters of the different configurations reported in the literature for interlayer water in bi-hydrated smectite layers.

Type I configuration[a]

Reference	Sample	Cation-$H_2O_{(iii)}$[b]	Cation-$H_2O_{(ii)}$[b]	Cation-$H_2O_{(i)}$[b]	B_{wat}[c, d]
Moore and Reynolds[1]	2W-Smectite	1.20	1.06	0.35	11/2[§]

Type II configuration

Reference	sample	O_{layer}-H_2O[b]	Cation-H_2O[b]	d_{001}[e]	$nH_2O/nCat$[f]	B_{wat}[c]
Mathieson et al.[51]	Mg-Vermiculite	2.76	1.14	14.34	-	5.4
Shirozu et al.[53]	Mg-Vermiculite	2.67[g]	1.17[g]	14.33	7.44	6.1
Alcover et al.[55]	Mg-Vermiculite	2.69	1.19	14.36	-	-
Le Renard et al.[60]	Altered Ca-Phlogopite	2.77	1.41	14.96	8.60	-
	Altered Na-Phlogopite	2.71	1.43	14.87	10.70	-
	Altered Li-Phlogopite	2.71	1.30	14.62	8.79	-
Beyer et al.[59]	Na-Vermiculite	2.70[g]	1.44[g]	14.85	4.00	3.9

Type III configuration

Reference	Sample	O_{layer}-H_2O[b,h]	Cation-H_2O[b,h]	d_{001}[e]	$nH_2O/nCat$[f]	B_{wat}[c]
De la Calle et al.[61]	Ca-Vermiculite	2.78	1.45[f]	14.92	7.34	5.5
Slade et al.[58]	Ca-Vermiculite	2.82	1.41[f]	14.89	8.02	2.5
	Na-Vermiculite	2.66	1.42	14.85	5.58	3.9

Type IV configuration

Reference	Sample	O_{layer}-H_2O[b]	O_{layer}-Cation[b]	Cation-H_2O[b]	d_{001}[e]	$nH_2O/nCat$[f]	B_{wat}[c]
Ben Brahim et al.[13]	Na-Beidellite	3.00	1.00	2.00	15.25	11.87	5

[a] Configurations of interlayer water in bi-hydrated smectite layers are schematized on Figure 2. [b] Distances are measured in projection along the c* axis and given in Å. O_{layer}, H_2O, and cation stand for the outermost plane of oxygen from the 2:1 layer, the H_2O molecules and the interlayer cations, respectively. [c] B_{wat} is the Debye-Waller temperature factor reported for H_2O molecules (in $Å^2$). [d] Debye-Waller factor is 11 $Å^2$ for plane (iii) and 2 $Å^2$ for planes (i) and (ii), respectively. [e] Basal distance d_{001} along the c* axis is given in Å. [f] $nH_20/nCat$ represents the ratio between the number of interlayer H_2O molecules and that of interlayer cations. [g] Average value for the different planes of H_2O molecules. [h] Distances are given for the denser plane of H_2O molecules.

Table 5. Distances along the c* axis between the interlayer mid-plane and the maximum density of the H_2O molecule distribution normalized to the thickness of the interlayer space for the different configurations of interlayer species.

Sample	2WS, B_{wat} = 2[a]	2WS, B_{wat} = 11[a]	2WG[b]
Ca-SWy-2 (40%RH)	27.8%[c]	30.1%	31.0%
Ca-SWy-1 (80%RH)	26.8%	29.4%	30.5%
Sr-SWy-1 (60%RH)	26.7%	29.4%	31.1%
Sr-SWy-1 (80%RH)	26.1%	30.7%	33.1%
Na-SWy-2 (80%RH)	26.7%	31.4%	33.4%
$Na\text{-}Sap_{0.8}$ (90%RH)	27.1%	30.0%	31.4%
$Na\text{-}Sap_{1.4}$ (90%RH)	28.4%	31.4%	31.9%
Mean value	27.1% ± 0.7%	30.3% ± 0.8%	31.8% ± 1.0%
Literature mean value[d]		32.7% ± 2.1%	

[a] 2WS corresponds to an interlayer configuration of H_2O molecules distributed as one plane on either side of the interlayer mid-plane. The Debye-Waller temperature factor for water (B_{wat}) given in $Å^2$. [b] 2WG corresponds to an interlayer configuration of H_2O molecules distributed according to a Gaussian function on either side of the interlayer mid-plane. [c] The distance along the c* axis between the interlayer mid-plane and the maximum density of the H_2O molecule distribution (Δd) is normalized to the thickness of the interlayer (L. Tck. minus the thickness of the 2:1 layer – 6.54 Å). [d] Average value calculated from the data reported for Type II and Type III configurations of interlayer species.[51,53,55,58-61]

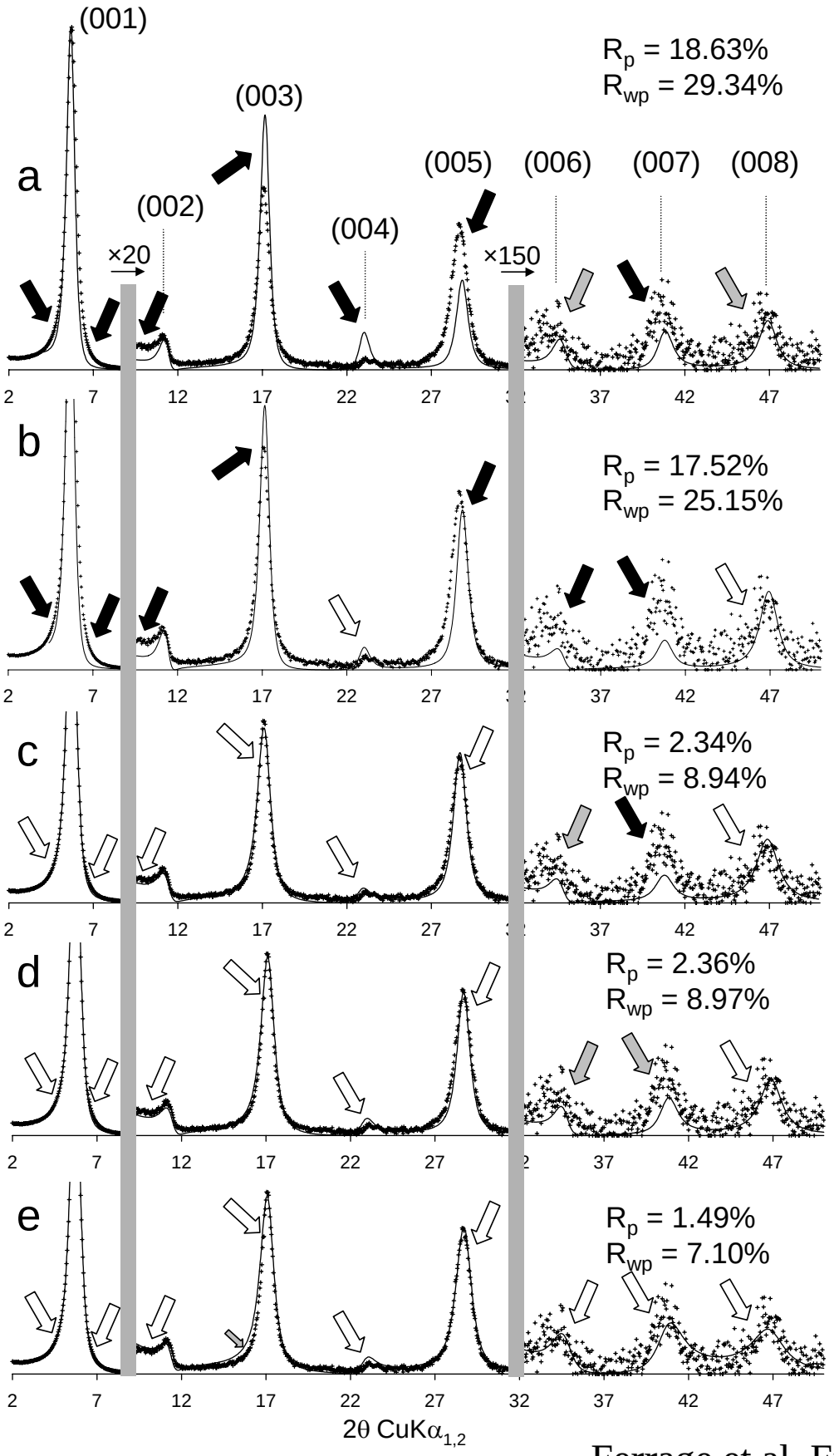

Ferrage et al. Fig. 01

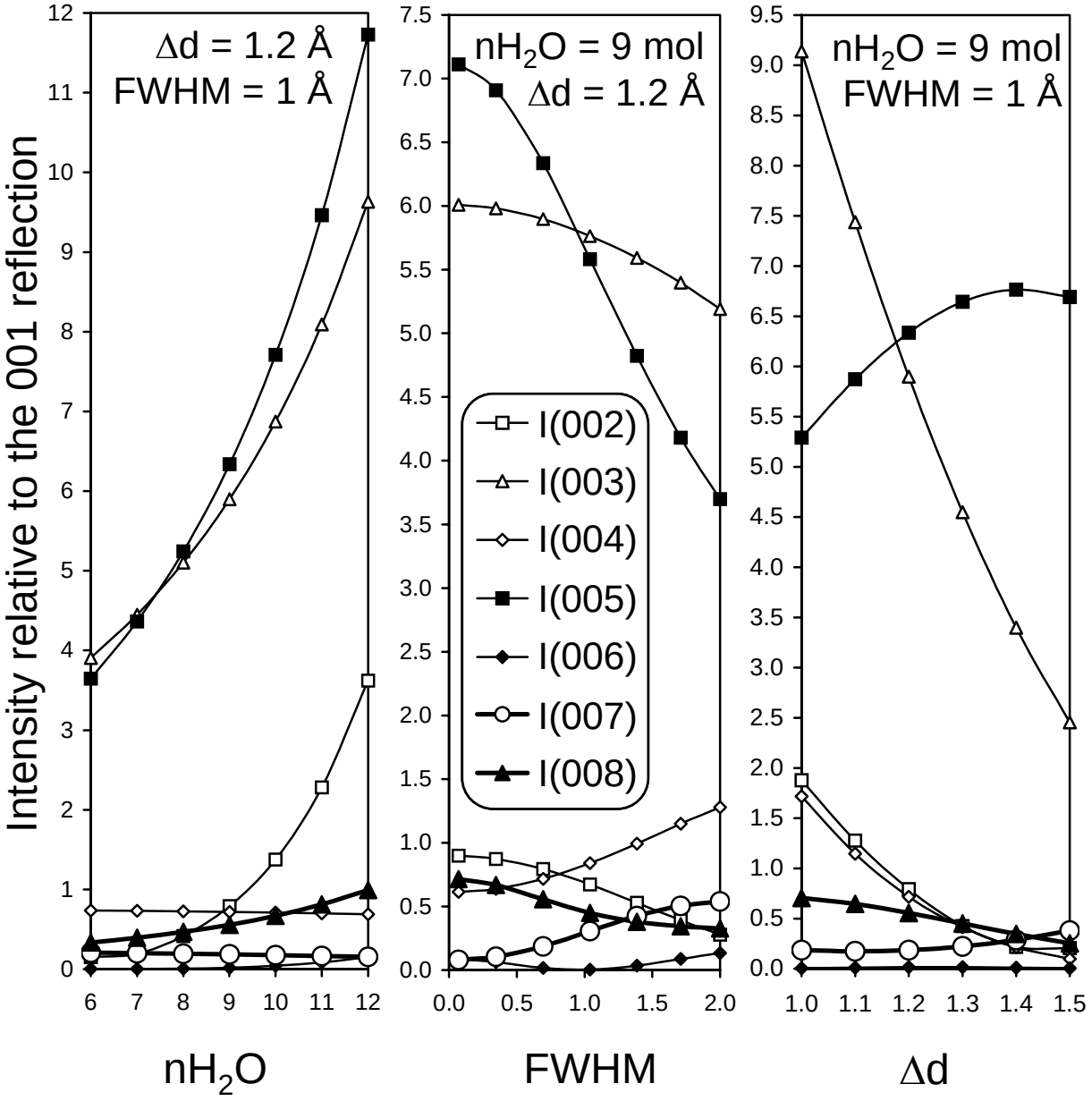

Ferrage et al. Fig. 02

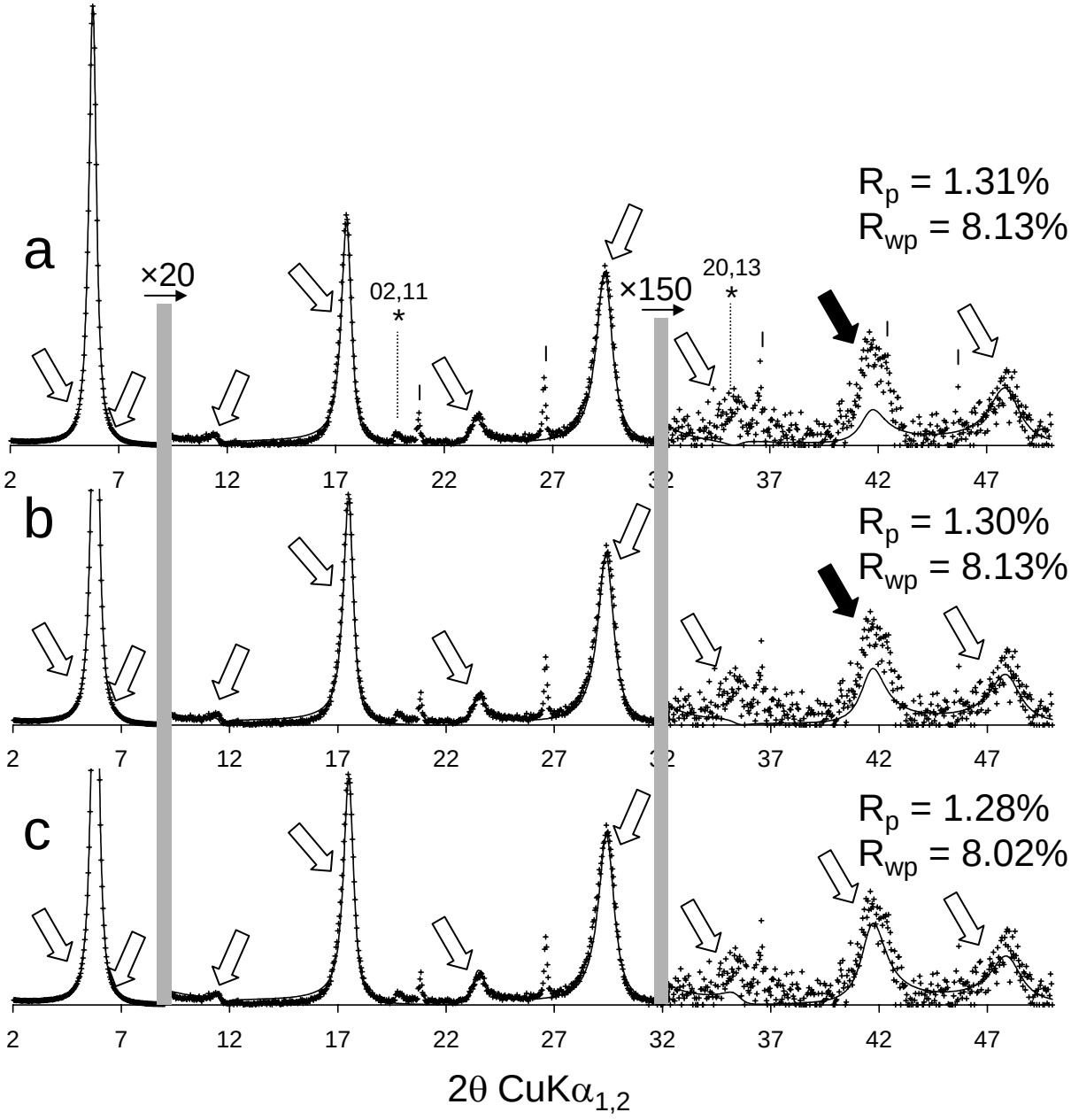

Ferrage et al. Fig. 03

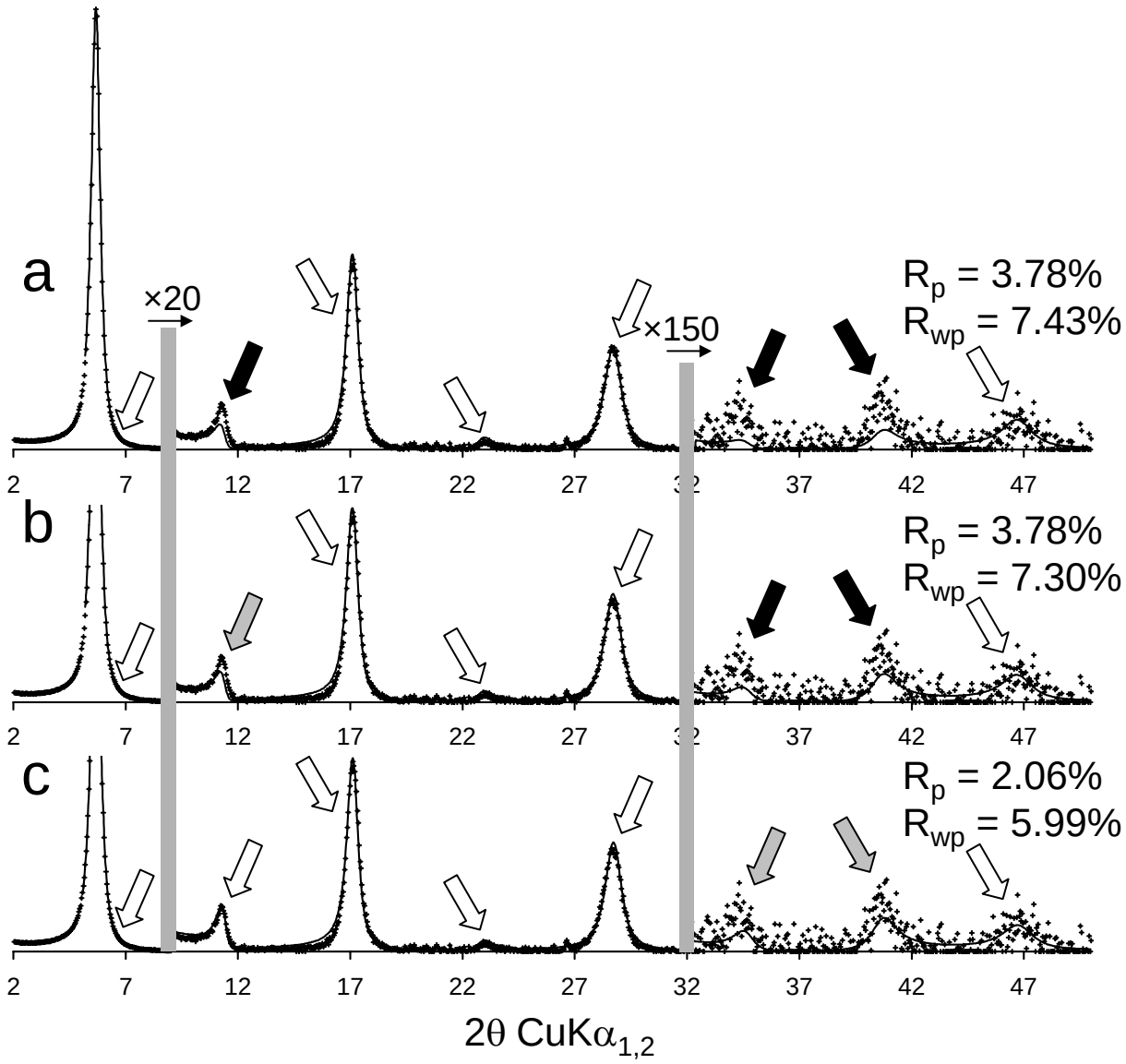

Ferrage et al. Fig. 04

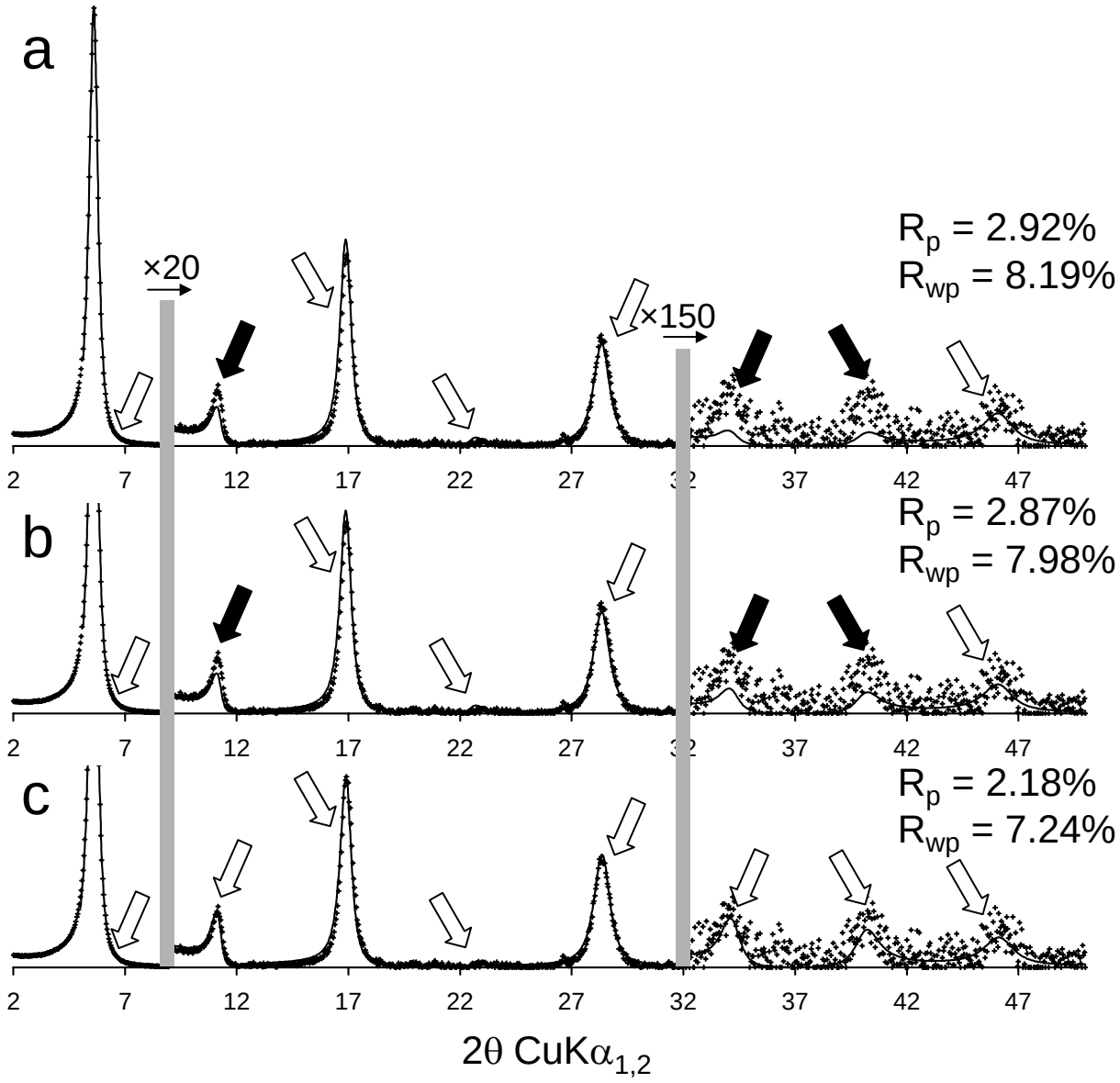

Ferrage et al. Fig. 05

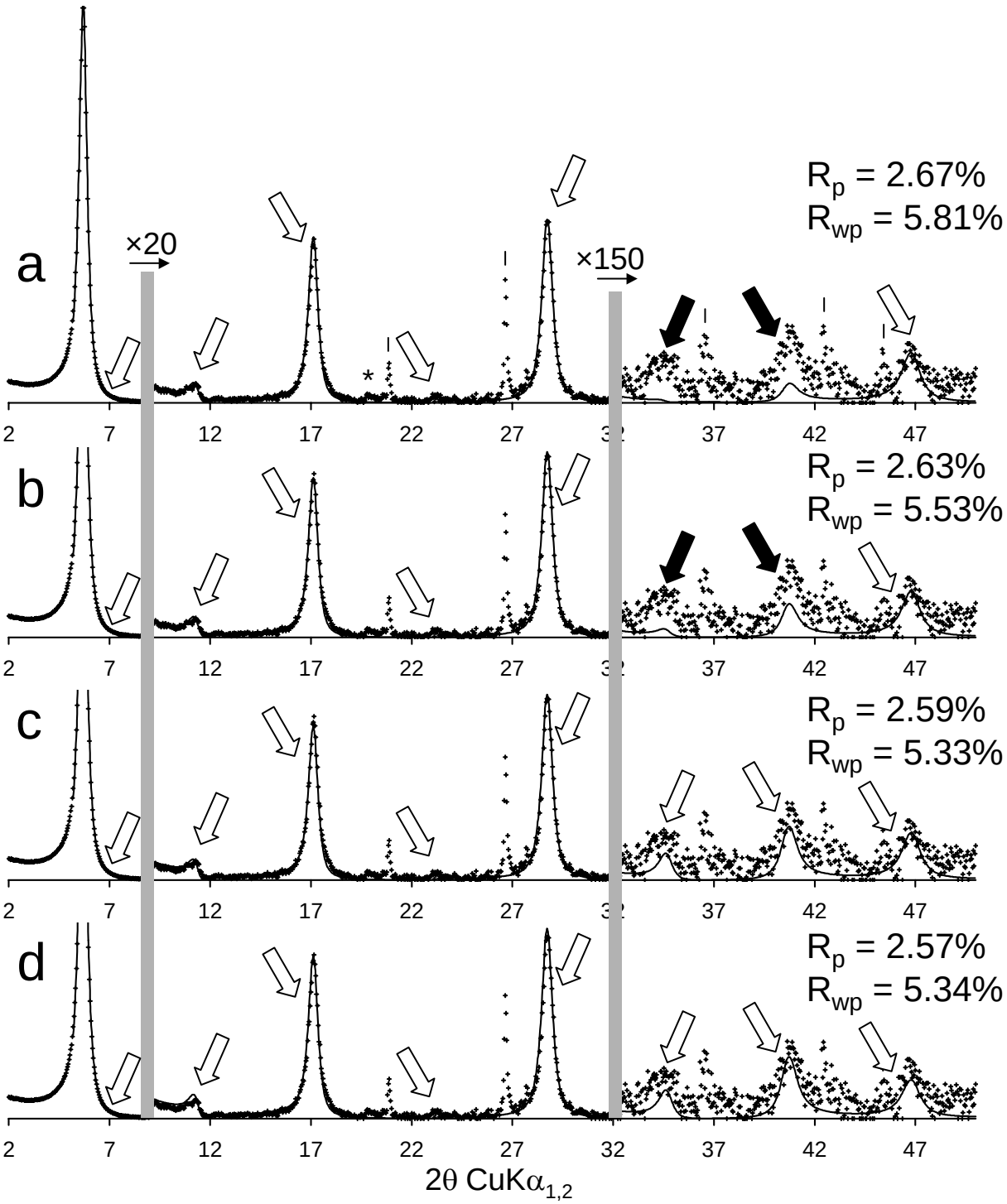

Ferrage et al. Fig. 06

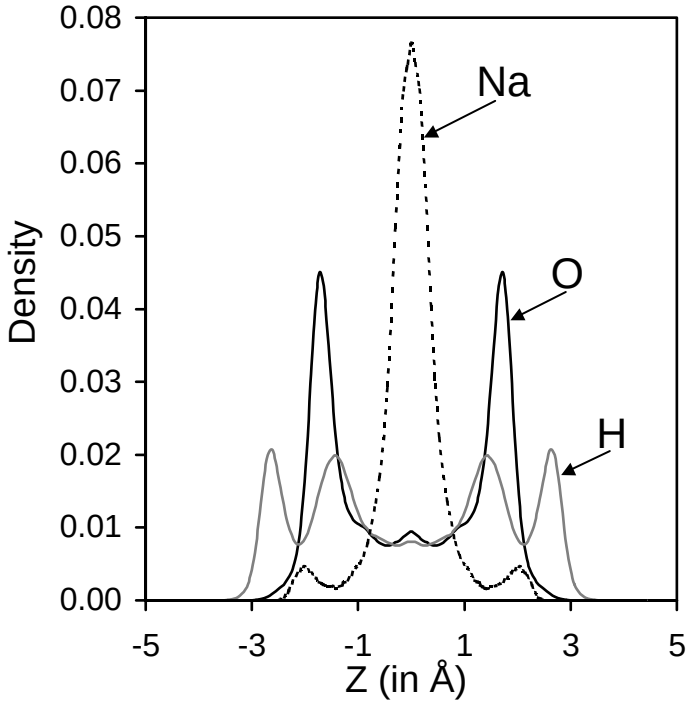

Ferrage et al. Fig. 07

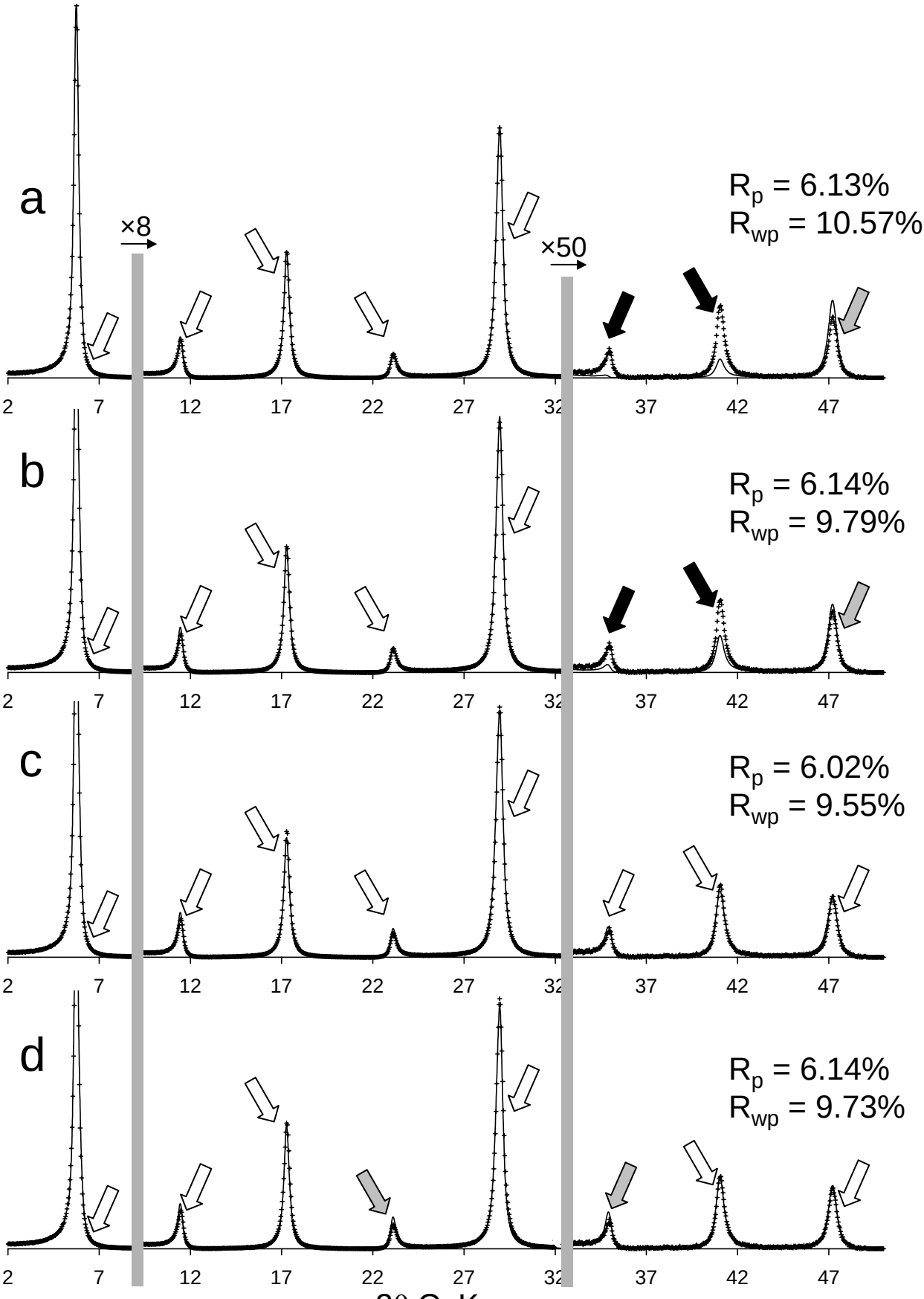

Ferrage et al. Fig. 08

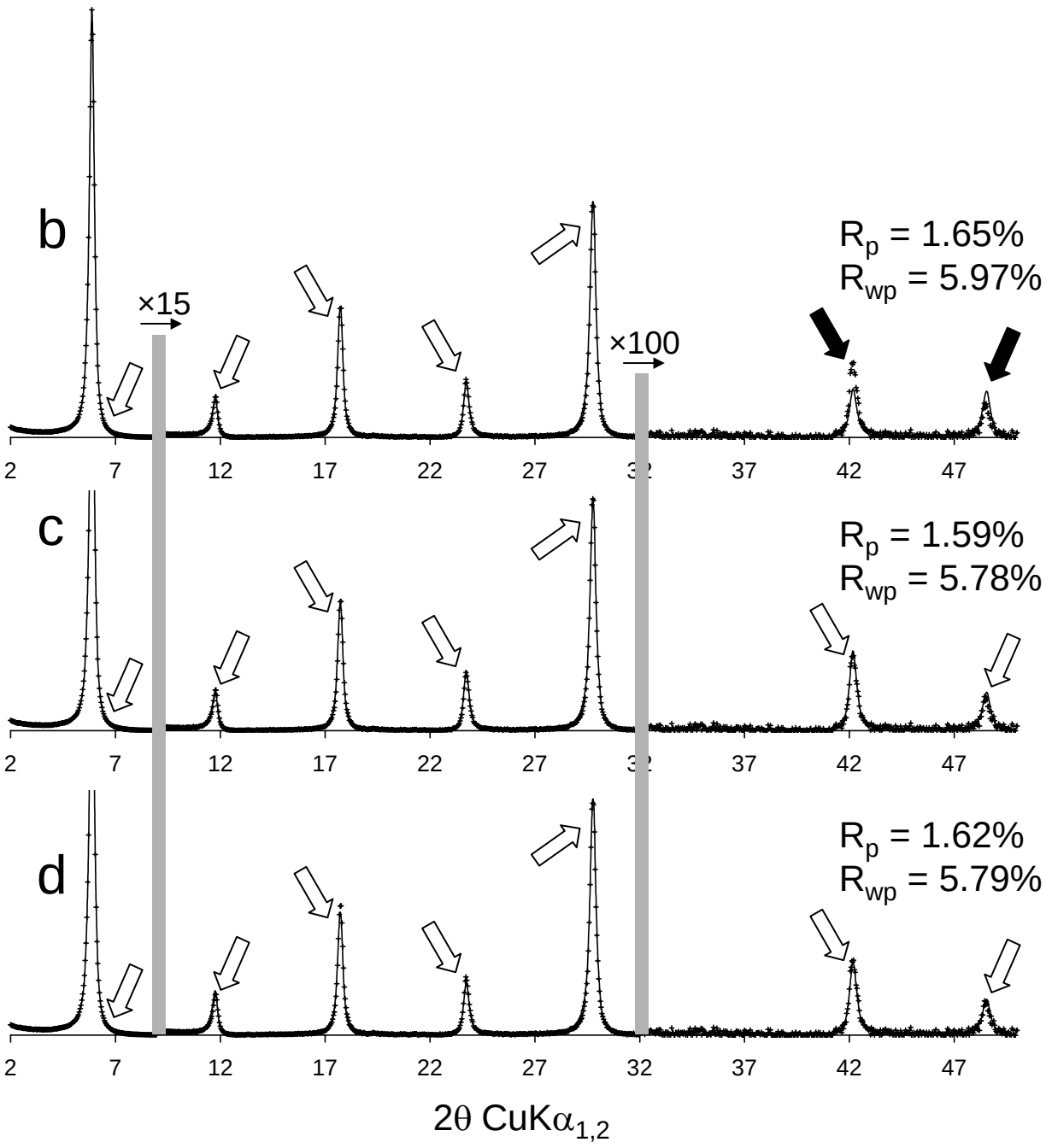

Ferrage et al. Fig. 09

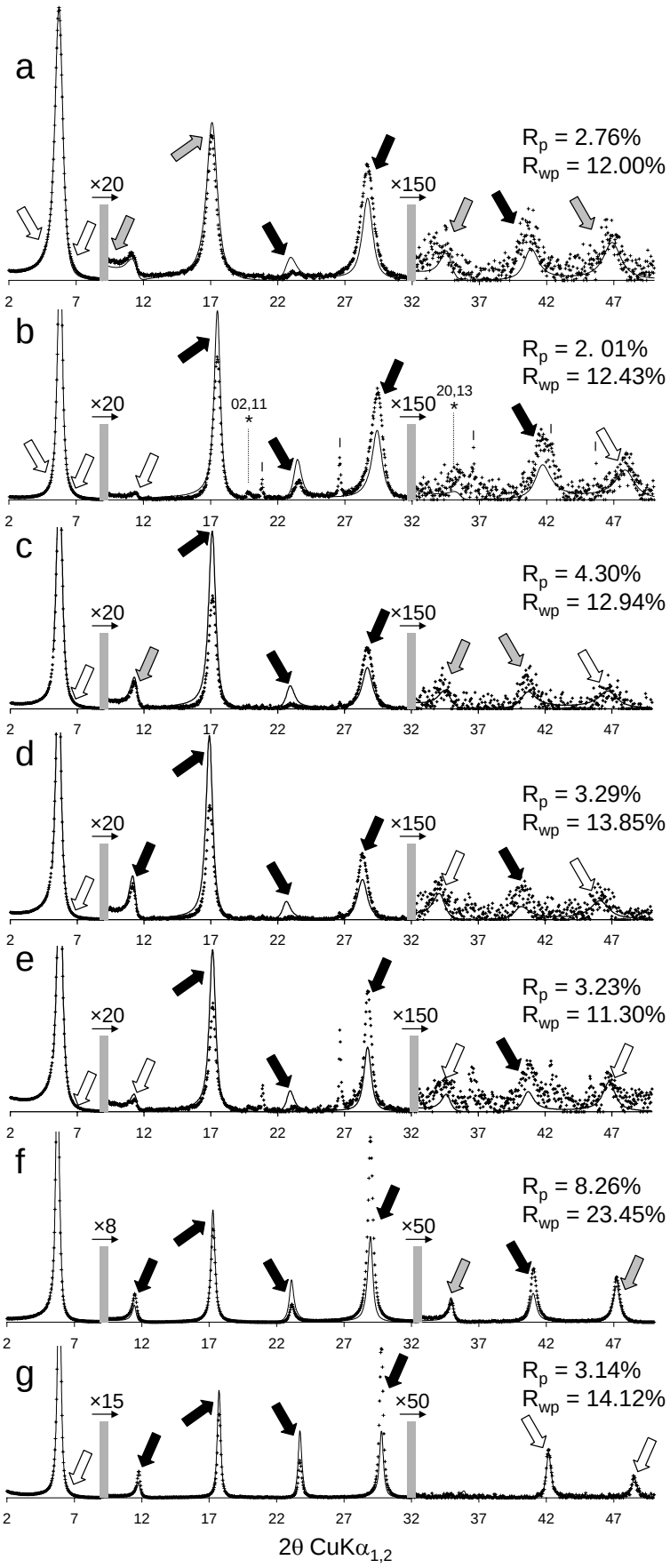

Ferrage et al. Fig. 10

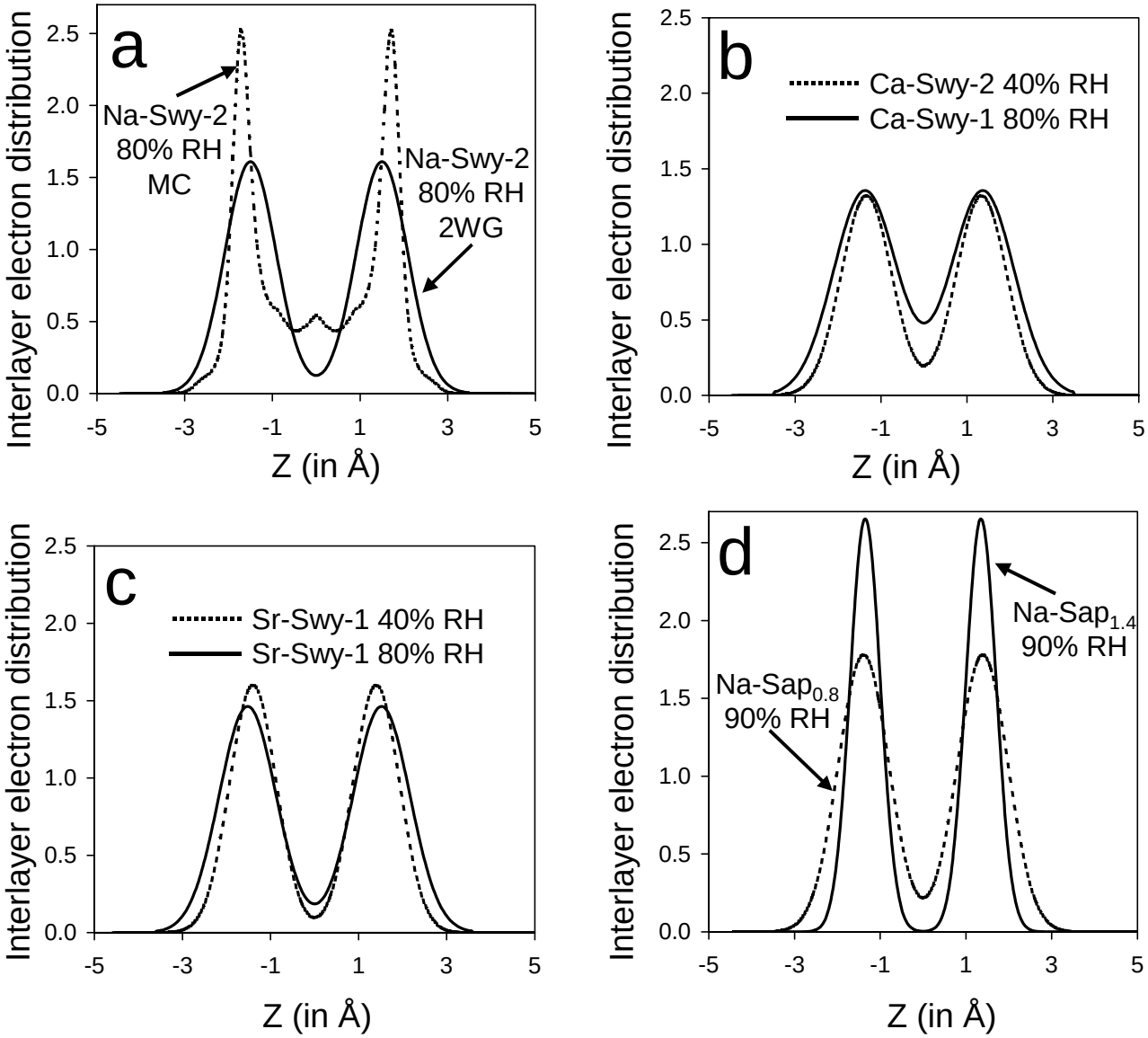

Ferrage et al. Fig. 11

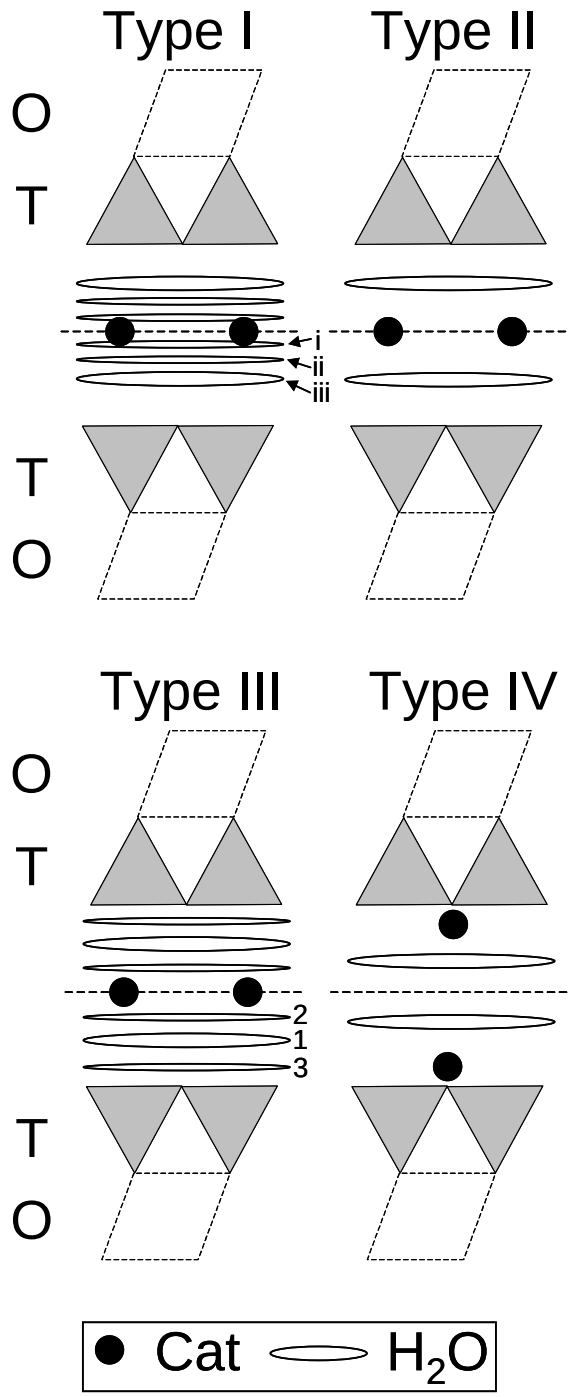

Ferrage et al. Fig. 12

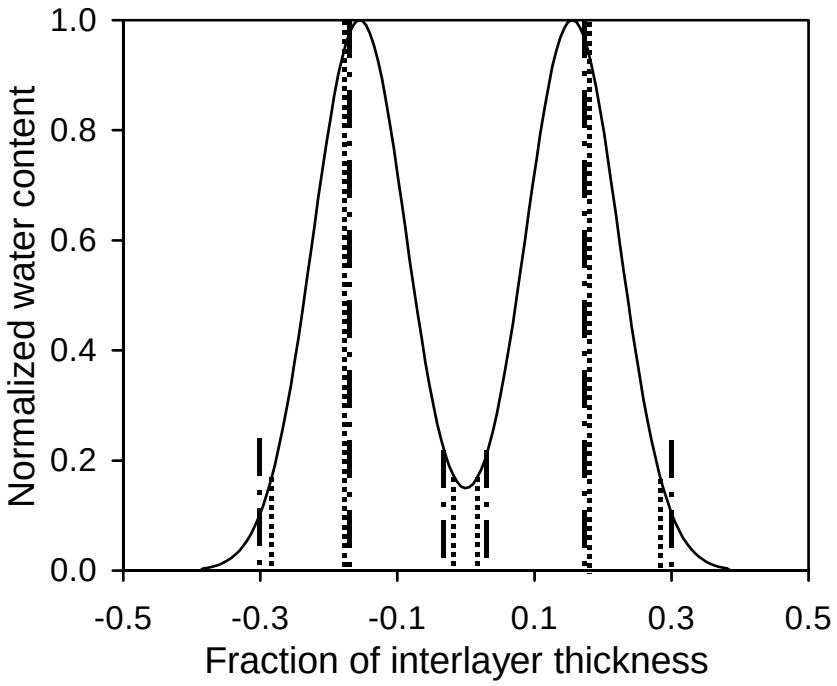

Ferrage et al. Fig. 13

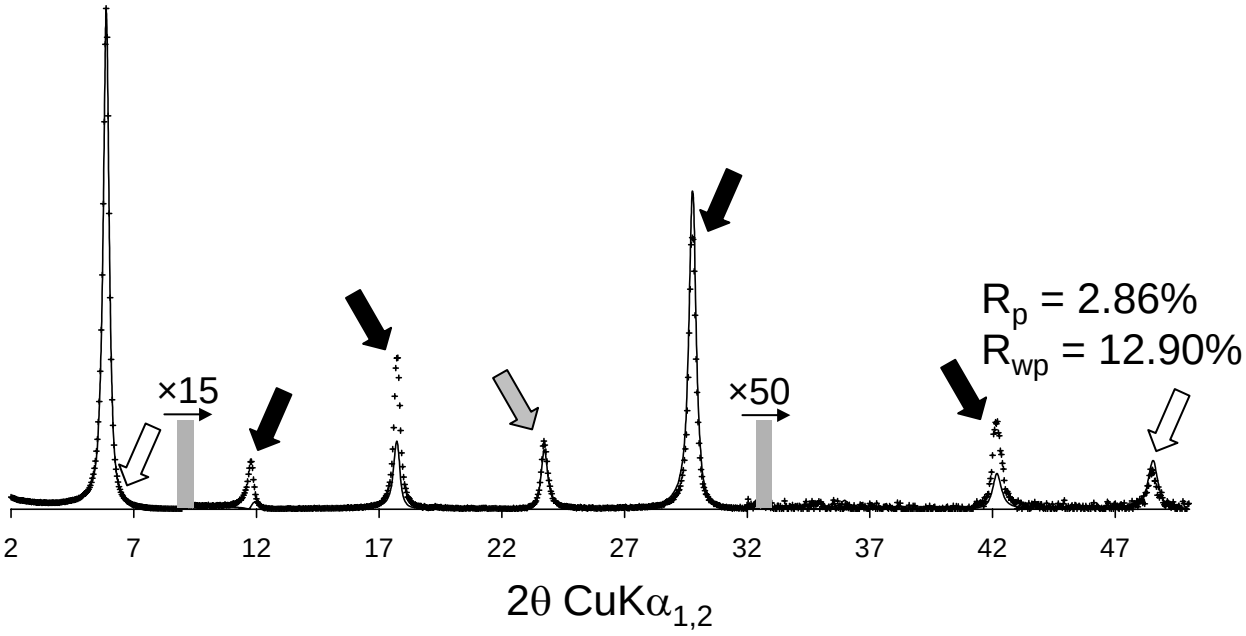

Ferrage et al. Fig. 14